

1    **Coccolithophore abundance and production and their impacts on particulate**  
2    **inorganic carbon cycling in the western North Pacific**

3    Yuye Han<sup>1,2</sup>, Zvi Steiner<sup>2</sup>, Zhimian Cao<sup>1\*</sup>, Di Fan<sup>3</sup>, Junhui Chen<sup>1</sup>, Jimin Yu<sup>3</sup> and Minhan Dai<sup>1\*</sup>

4    <sup>1</sup>State Key Laboratory of Marine Environmental Science & College of Ocean and Earth Sciences, Xiamen University, Xiamen,  
5    China

6    <sup>2</sup>Marine Biogeochemistry Division, GEOMAR Helmholtz Centre for Ocean Research, Kiel, Germany

7    <sup>3</sup>Laoshan Laboratory, Qingdao, China

8  
9    *Correspondence to:* mdai@xmu.edu.cn & zmcao@xmu.edu.cn

10 **Abstract.** Coccolithophores are globally distributed, calcifying phytoplankton that play an important role in the marine carbon  
11 cycle through their contribution to the carbonate pump. However, limited knowledge of their biogeography and environmental  
12 drivers hinders our ability to predict the response of the marine carbonate pump to climate change. Here we investigated  
13 coccolithophore abundance, species composition, coccolithophore-derived calcium carbonate ( $\text{CaCO}_3$  as calcite), and  
14 particulate inorganic carbon (PIC) concentrations in the upper water column of the western North Pacific Ocean. Sampling  
15 was conducted along a meridional transect spanning the oligotrophic subtropical gyre and the nutrient-rich Kuroshio-Oyashio  
16 transition region. Our results show that *Umbellosphaera tenuis* is the numerically dominant coccolithophore species in the  
17 subtropical gyre, while *Emiliania huxleyi* and *Syracosphaera* spp. dominated in the transition region. The coccolithophore  
18 community composition exhibited significant depth- and latitude-dependent variations. On average, coccolithophore calcite  
19 contributed  $79 \pm 27$  % of the total  $\text{CaCO}_3$  standing stock in Niskin bottle samples from the euphotic zone, with a higher  
20 contribution observed in the subtropical gyre ( $91 \pm 30$  %) compared to the Kuroshio-Oyashio transition region ( $70 \pm 24$  %).  
21 This pattern was further supported by size-fractionated PIC data from in situ pump samples, with the small-size fraction (1–  
22  $51 \mu\text{m}$ ) contributing  $76 \pm 11$  % of the total PIC ( $> 1 \mu\text{m}$ ) in the subtropical gyre, compared to  $67 \pm 13$  % in the transition region.  
23 During the sampling period, coccolithophore  $\text{CaCO}_3$  production rate ranged from 0.8 to  $2.1 \text{ mmol m}^{-2} \text{ d}^{-1}$ , averaging  $1.5 \pm 0.7$   
24  $\text{mmol m}^{-2} \text{ d}^{-1}$  in the subtropical gyre and  $1.2 \pm 0.4 \text{ mmol m}^{-2} \text{ d}^{-1}$  in the transition region. These findings highlight the critical  
25 role of coccolithophores in the pelagic  $\text{CaCO}_3$  cycle, particularly in oligotrophic ocean waters, and emphasize the need for  
26 improved mechanistic understanding of their distribution and calcification dynamics in a changing ocean.

## 27 **1 Introduction**

28 Calcium carbonate ( $\text{CaCO}_3$ ) production and dissolution comprise  $\text{CaCO}_3$  cycling in the ocean, and are a key component of the  
29 global oceanic carbon cycle (Broecker and Peng, 1982) through the carbonate pump (Volk and Hoffert, 1985). Production of  
30 biogenic  $\text{CaCO}_3$  by calcifying plankton in the euphotic zone elevates the partial pressure of carbon dioxide ( $\text{CO}_2$ ) in seawater  
31 (e.g., Feely et al., 2002), while ballasting of sinking particles can promote the transport of carbon from the surface to deep sea  
32 and marine sediments (e.g., Armstrong et al., 2001; Klaas and Archer, 2002). Dissolution of  $\text{CaCO}_3$  in the water column acts  
33 as a buffer to facilitate ocean sequestration of atmospheric  $\text{CO}_2$  and reduces the rate of ocean acidification (Feely et al., 2004;  
34 Barrett et al., 2014). Over the last decade, ocean acidification, a global reduction in seawater pH caused by the uptake of  
35 anthropogenic  $\text{CO}_2$ , has emerged as a significant feedback mechanism, making it harder for calcifying organisms to produce  
36 their skeletons, and thus adversely affects marine ecosystems (Feely et al., 2004; Ma et al., 2023). Therefore, quantification of  
37 marine  $\text{CaCO}_3$  production and dissolution is of vital importance in determining the response of marine ecosystems to changes  
38 in the partial pressure of  $\text{CO}_2$ .

39 Marine  $\text{CaCO}_3$  occurs in the form of calcite, aragonite and high-magnesium calcite. Coccolithophores are a key, single-  
40 celled phytoplankton taxonomic group, responsible for a large percentage (30–60 %) of modern oceanic  $\text{CaCO}_3$  production  
41 and 10–20 % of marine primary production on a global scale (Poulton et al., 2006, 2013). Coccolithophore calcite accounts  
42 for a major fraction (24–80 %) of the  $\text{CaCO}_3$  exported to the deep sea and sediments (Broerse et al., 2000; Young and Ziveri,  
43 2000; Rigual Hernández et al., 2020). Field observations along a northeast Pacific transect from Hawaii to Alaska suggested  
44 that coccolithophore calcite comprises 90 % of the total  $\text{CaCO}_3$  production in the euphotic zone, while pteropods and  
45 foraminifera only play a minor role (Ziveri et al., 2023). However, large uncertainties remain in estimates of the production  
46 rate of  $\text{CaCO}_3$  in the upper ocean, as well as the contributions of different plankton groups, which are still unclear and vary  
47 across regions (Balch et al., 2007; Berelson et al., 2007; Smith and Mackenzie, 2016; Ziveri et al., 2023). Based on a global  
48 compilation of  $\text{CaCO}_3$  production using in situ  $^{14}\text{C}$  incubations, Daniels et al. (2018) found that calcification rate ranged from  
49  $<0.1$  to  $6 \text{ mmol m}^{-2} \text{ d}^{-1}$  in the euphotic zone. A recent estimate of  $\text{CaCO}_3$  biomass from three main pelagic calcifying plankton  
50 groups also suggested large variation in  $\text{CaCO}_3$  production in the eastern North Pacific Ocean, ranging from 1.1 to  $7.3 \text{ mmol}$   
51  $\text{m}^{-2} \text{ d}^{-1}$  (Ziveri et al., 2023).

52 The North Pacific Ocean is a vital region for modulating the carbon cycle, as it accounts for ~25 % of the global ocean sink  
53 for atmospheric CO<sub>2</sub> (Takahashi et al., 2009). In the eastern North Pacific Ocean, CaCO<sub>3</sub> production, export, and dissolution  
54 have been studied along a transect from Hawaii to Alaska (Dong et al., 2019, 2022; Naviaux et al., 2019; Subhas et al., 2022;  
55 Ziveri et al., 2023). Ziveri et al. (2023) found that depth-integrated CaCO<sub>3</sub> production in the nutrient-rich subpolar gyre is  
56 twice as high as that in the nutrient-poor subtropical gyre. This contrast, however, is smaller than the sixfold to sevenfold  
57 difference based on satellite estimates of surface particulate inorganic carbon (PIC), indicating the importance of  
58 coccolithophore CaCO<sub>3</sub> production over a deeper euphotic zone and the limitation of satellite products as highlighted by  
59 Neukermans et al. (2023).

60 Here, we determined the abundance and species composition of coccolithophores, as well as the concentrations of  
61 coccolithophore calcite and PIC based on both Niskin bottle and in situ pump sampling in the upper water column of the  
62 western North Pacific Ocean. Additionally, we conducted measurements of environmental conditions such as nutrient and  
63 carbonate chemistry parameters. The aims of this research were to answer the following questions: (1) What is the distribution  
64 of coccolithophore abundances and species compositions across the oligotrophic-nutrient replete environmental gradient? (2)  
65 What is the contribution of coccolithophores to CaCO<sub>3</sub> production in the euphotic zone?

66

## 67 **2 Methods**

### 68 **2.1 Sample collection**

69 Sampling was conducted onboard R/V *Tan Kah Kee* during cruise NORC2022-306 from 09 June to 25 July 2022. The cruise  
70 trajectory crossed from the oligotrophic North Pacific Subtropical Gyre (NPSG) to the relatively nutrient-rich Kuroshio-  
71 Oyashio transition region along the 155°E meridian (Fig. 1a; Table S1). Seven sampling stations can be divided into those  
72 located in the NPSG region, including stations M30, M32 and M35, characterized by high sea-surface temperature (SST) and  
73 low surface chlorophyll *a* (Chl *a*) and PIC concentrations, and those located in the Kuroshio-Oyashio transition region,  
74 including stations KE3, STN41, STN43 and STN45, featuring lower SST, but higher Chl *a* and PIC concentrations (Fig. 1b–  
75 d).

76

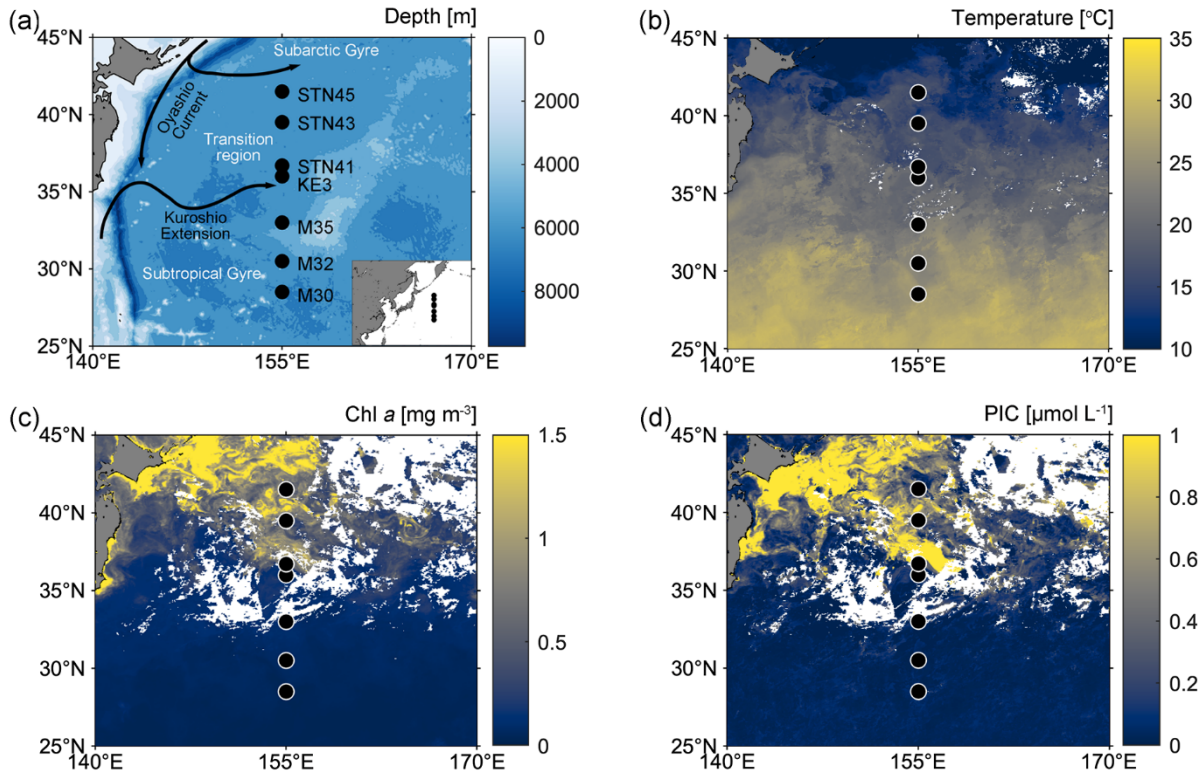


**Fig. 1.** (a) Map of the western North Pacific Ocean showing sampling stations (black filled circles) and major surface currents (solid black lines); (b–d) satellite-based temperature, chlorophyll *a* (Chl *a*) and particulate inorganic carbon (PIC) concentrations in surface water from 1<sup>st</sup> to 30<sup>th</sup> June 2022 (data from the Moderate Resolution Imaging Spectroradiometer (MODIS)-Aqua satellite; <https://oceancolor.gsfc.nasa.gov/13/>).

Water samples were collected within the water column above 300 m depth using Niskin bottles on a rosette system equipped with SBE-911 conductivity-temperature-depth (CTD) sensors (Sea-Bird Electronics, Inc., Bellevue, WA, USA). For PIC analyses, 24 L of seawater were collected using acid-cleaned fluorinated bottles and filtered through two quartz microfiber (QMA) filters (1.0 μm pore size, 25 mm diameter). For coccolithophore analyses, 2–4 L of seawater were collected and gently filtered through polycarbonate membranes (0.8 μm pore size, 25 mm diameter), using a vacuum pump at <20 mm Hg pressure. Membrane filters were oven-dried at 60°C and stored in plastic petri dishes.

89 Size-fractionated particles were collected using McLane Research in situ pumps. Filter holders were loaded with a 51  $\mu\text{m}$   
90 Sefar polyester mesh prefilter followed by paired Whatman QMA filters. Hereafter, we refer to the two particle size fractions  
91 as large ( $> 51 \mu\text{m}$ ) and small ( $1\text{--}51 \mu\text{m}$ ) size fractions. A 1/4 subsample of the 51  $\mu\text{m}$  polyester mesh prefilter and two circles  
92 of 23 mm diameter subsample of the QMA filter were analyzed for large and small PIC concentrations, respectively, and the  
93 sum of the two fractions yielded the total (size fraction of  $> 1 \mu\text{m}$ ) PIC concentration.

## 94 **2.2 Sample analyses**

95 PIC concentrations were determined by measuring the amount of  $\text{CO}_2$  released after acid treatment of the filters using a Thermo  
96 Delta V Plus isotope ratio mass spectrometer (IRMS, Thermo Fisher, USA) coupled with a Thermo Gasbench II system at the  
97 Center for Isotope Geochemistry and Geochronology of the Laoshan Laboratory (Li et al., 2021). International reference  
98 materials of calcite NBS-18 and IAEA-603 were measured for calibration. The analytical precision of PIC determination was  
99  $<10\%$  (one standard deviation, 1SD).

100 Filters were cut and mounted with a carbon sticky tab on a stub and gold-coated prior to analysis using a Quanta 650 FEG  
101 field-emission scanning electron microscope (SEM). The coccosphere cell or detached coccolith concentrations (CC, cells or  
102 coccoliths  $\text{L}^{-1}$ ) were estimated as follows:

$$103 \text{ CC} = (F * C)/(V * S) \quad (1)$$

104 where F is the effective filtration area ( $336.9 \text{ mm}^2$ ), C is the total number of coccosphere cells or detached coccoliths, V is the  
105 filtered seawater volume, and S is the total area of fields of view ( $\text{mm}^2$ ). This cell counting strategy gives a detection limit of  
106 at least  $1.87 \text{ cells mL}^{-1}$  (Bollmann et al., 2002). The coccolithophore abundance in four samples, that were collected at 10 m  
107 and 200 m at station M30, 200 m at station KE3 and 200 m at station STN45, fell below the detection limit. Despite potential  
108 inaccuracies, these values are still meaningful as they indicate an exceptionally low coccolithophore presence. Coccolithophore  
109 species identification followed Young et al. (2003) and the Nannotax3 website (<http://ina.tmsoc.org/Nannotax3/>). Aggregates  
110 formed by clusters of multiple coccolithophores were quantified in terms of abundance but were excluded from the  
111 coccolithophore calcite calculations, mainly due to the difficulty in accurately determining the number of individual coccoliths  
112 within the aggregates. Individual coccolithophore calcite content was calculated by multiplying the number of coccoliths per  
113 cell by the average coccolith calcite mass of a given species. The average coccolith mass was estimated based on the coccolith

size (usually using coccolith length) and a factor related to coccolith cross-sectional shape (Young and Ziveri, 2000):

$$m \text{ (pg CaCO}_3\text{)} = 2.7 * K_s * l^3 \quad (2)$$

where  $l$  is the coccolith size ( $\mu\text{m}$ ),  $K_s$  is a species-specific shape constant, and 2.7 is the calcite density ( $\text{CaCO}_3$ ;  $\text{pg } \mu\text{m}^{-3}$ ). The specific coccolith distal shield length or process height used in the calculation was measured from SEM images. Measurements were conducted using ImageJ free software ([imagej.nih.gov/ij/](http://imagej.nih.gov/ij/)) and Coccobiom2-SEM measuring macro (Young, 2015). The  $K_s$  values used were from Young and Ziveri (2000) and Jin et al. (2016). The number of coccoliths per coccosphere was obtained from Yang and Wei (2003) and Boeckel and Baumann (2008). The calculation of coccolith PIC is detailed in Table S2 in the Supplement. Sheward et al. (2024) have extensively discussed the potential errors of the morphometric-based calcite estimation method, suggesting that an additional uncertainty of 5–40 % may arise from slight variations in  $K_s$  and size between coccoliths on the same coccosphere, as well as errors in coccolith number estimation. Additionally, it is important to note that further uncertainties can be introduced by counting inaccuracies, particularly in cases where clumps or overlapping coccoliths are present. Despite these possible errors and limitations, our data and results offer robust and comparable insights into coccolithophore calcite dynamics.

Chl  $a$  concentrations were measured after being extracted with 90 % acetone for 14 h at  $-20^\circ\text{C}$  using a Trilogy Laboratory Fluorometer with non-acidification module (Turner Designs, USA) (Welschmeyer, 1994). Nutrient samples were collected in acid-washed Nalgene high-density polyethylene bottles and determined onboard the vessel using a Four-channel Continuous-Flow Technicon AA3 Autoanalyzer (Bran+Luebbe GmbH). The detection limits were  $0.1 \mu\text{mol L}^{-1}$ ,  $0.08 \mu\text{mol L}^{-1}$ , and  $0.16 \mu\text{mol L}^{-1}$  for dissolved inorganic nitrogen (DIN, nitrate plus nitrite), soluble reactive phosphate (SRP), and dissolved silicate (DSi), respectively. The analytical precisions (derived from repeat measurements of aged deep seawater) were 0.44% for DIN, 0.91% for SRP, and 0.28% for DSi ( $n = 82$ ). Analysis of reference standard LOT.CM (KANSO TECHNOS CO., LTD.) produced concentrations of  $33.72 \pm 0.13 \mu\text{mol L}^{-1}$  for DIN,  $2.460 \pm 0.025 \mu\text{mol L}^{-1}$  for SRP, and  $102.2 \pm 0.3 \mu\text{mol L}^{-1}$  for DSi ( $n = 20$ ), which agree well with consensus values ([http://www.kanso.co.jp/eng/pdf/certificate\\_cb.pdf](http://www.kanso.co.jp/eng/pdf/certificate_cb.pdf)). For measurements of DIN and SRP concentrations in surface samples below the detection limit of the AA3 Autoanalyzer, duplicate samples were collected and frozen separately at  $-20^\circ\text{C}$  until analysis. Nanomolar DIN concentrations were determined using a continuous-flow analysis system combined with a liquid waveguide capillary flow cell as described by Zhang (2000). The detection limit

139 was 5.2 nmol L<sup>-1</sup> and the analytical precision was 7.5% (derived from repeat measurements of aged deep seawater with 1000-  
140 fold dilution, 36.2 ± 2.7 nmol L<sup>-1</sup>, n = 57). Nanomolar SRP concentrations were measured using an automated analyzer  
141 including a syringe pump and multiposition selection valve combined with a solid-phase extraction cartridge (Deng et al.,  
142 2020). The detection limit was 2.5 nmol L<sup>-1</sup> and the analytical precision was 5% (derived from repeat measurements of aged  
143 deep seawater with 1000-fold dilution, 26.0 ± 1.2 nmol L<sup>-1</sup>, n = 56). Seawater ammonium (NH<sub>4</sub><sup>+</sup>) concentrations were  
144 measured onboard using solid-phase extraction combined with fluorescence determination with a detection limit of 3.6 nmol  
145 L<sup>-1</sup> (Zhu et al., 2013, 2018).

146 Samples for analysis of dissolved inorganic carbon (DIC) and total alkalinity (TA) were collected in 250 mL PYREX®  
147 borosilicate glass bottles, and poisoned with 250 µL of a HgCl<sub>2</sub>-saturated solution upon sample collection. DIC was measured  
148 using an infrared CO<sub>2</sub> detector (Apollo ASC-3) , with a precision of ± 2 µmol L<sup>-1</sup> (Cai et al., 2004). TA was determined on 25  
149 mL samples using an open-cell setting based on the Gran titration technique (Cai et al., 2010) with a Kloehn digital syringe  
150 pump. The analytical precision was ± 2 µmol L<sup>-1</sup>. Both DIC and TA concentrations were calibrated against certified reference  
151 materials provided by Andrew G. Dickson (the Scripps Institution of Oceanography, University of California, San Diego,  
152 USA).

### 153 **2.3 Estimation of CaCO<sub>3</sub> production rate**

154 The euphotic zone bottom at each station was defined as the depth where surface photosynthetically active radiation (PAR)  
155 reaches 0.1 % (Table S1). CaCO<sub>3</sub> production rates in the euphotic zone were determined by dividing measurements of the  
156 living CaCO<sub>3</sub> standing stock (which only included whole coccosphere cells and excluded loose coccoliths) by the  
157 coccolithophore turnover time, which is 0.7–10 days with a growth rate ranging from 0.1 to 1.5 cell divisions day<sup>-1</sup> (Krumhardt  
158 et al., 2017; Ziveri et al., 2023). The coccolithophore turnover time was derived from both laboratory and field estimates, as  
159 well as simulations from a generalized coccolithophore model, which has also been applied to the eastern North Pacific Ocean  
160 (Krumhardt et al., 2017; Ziveri et al., 2023). We are aware that different coccolithophore species exhibit widely varying growth  
161 rates and cell growth phase differs. Smaller cells produce fewer coccoliths during the exponential growth phase characterized  
162 by rapid division, whereas larger cells generate more coccoliths during the early stationary phase when cell division slows  
163 down (Raven and Crawford, 2012; Krumhardt et al., 2017). We also acknowledge that estimating coccolithophore calcite and



164 production rates using an average coccolith calcite value introduces uncertainties, as this approach does not fully account for  
165 the complexity of coccolith dynamics, including rapid cycling and reabsorption (Johns et al., 2023). Despite these possible  
166 errors and uncertainties, our estimations generally comparable with those of prior work (e.g., Daniels et al., 2018), remain a  
167 reliable basis for assessing coccolithophore calcification. Uncertainty in the  $\text{CaCO}_3$  standing stock estimates, which were  
168 obtained by vertically integrating PIC concentrations in the euphotic zone, was typically  $\pm 10\%$  (1SD).

169 A Monte Carlo-based probabilistic approach was used to determine the  $\text{CaCO}_3$  production rate and the uncertainties  
170 associated with the turnover time using the R package vioplot. To obtain an annual  $\text{CaCO}_3$  production based on our field  
171 observations, we used the ratio of satellite-derived PIC for July 2022 to annual climatology PIC (data from the NASA Goddard  
172 Space Flight Center's Ocean Ecology Laboratory) to calibrate for potential seasonal variability (Ziveri et al., 2023).

## 173 **2.4 Influence of environmental conditions on coccolithophores**

174 The redundancy analysis (RDA) is a widely used multivariate analytical method to identify relationships among individual  
175 variables in different categories. Prior to the RDA, statistical differences in environmental variables were evaluated using an  
176 analysis of variance (one-way ANOVA), while collinearity between environmental variables was accounted for by calculating  
177 variance inflation factors (VIF). Forward selection of variables was subsequently carried out until all VIF scores were  $<10$ , in  
178 order to only including variables that are not significantly correlated. These criteria reduced the number of environmental  
179 variables used in the RDA. Monte Carlo permutation tests, based on 1000 randomizations, were performed to identify the most  
180 significant and independent effect on variation in the coccolithophore community composition. The overall significance of the  
181 explanatory variables after forward selection was evaluated through ANOVA ( $\alpha < 0.05$ ) and coefficient of determination ( $r^2$ ),  
182 and adjusted  $r^2$  were calculated to assess the power of a selected RDA model using the vegan package (Oksanen, 2010). The  
183 contribution of each environmental variable to community variation was determined by hierarchical partitioning in canonical  
184 analysis via the 'dbRDA' function in the "rdacca.hp" package in R (Lai et al., 2022).

185

## 186 **3 Results**

### 187 **3.1 Hydrography**

188 Hydrochemical variables exhibited a south to north trend. Temperature and salinity were highest at the surface of station M30,

189 due to strong net evaporation in the subtropical gyre (Fig. 2a and b). There was a northward decrease in temperature and  
190 salinity due to the influence of upwelling in the subarctic gyre. In contrast to temperature and salinity and as expected, the  
191 distribution of DIN, SRP and DSi showed a generally northward increasing pattern (Figs. 2c–d and S1a). Surface DIN  
192 concentrations were on average  $0.006 \mu\text{mol L}^{-1}$  in the NPSG region and  $0.02 \mu\text{mol L}^{-1}$  in the Kuroshio-Oyashio transition  
193 region. The  $\text{NH}_4^+$  concentration above 100 m at station STN45 was notably higher than that at other stations (Fig. S1b). The  
194 deep chlorophyll maximum (DCM) depth gradually shoaled northward from 110 m at station M30 in the NPSG region to 33  
195 m at station STN45 in the Kuroshio-Oyashio transition region (Fig. 2e).

196

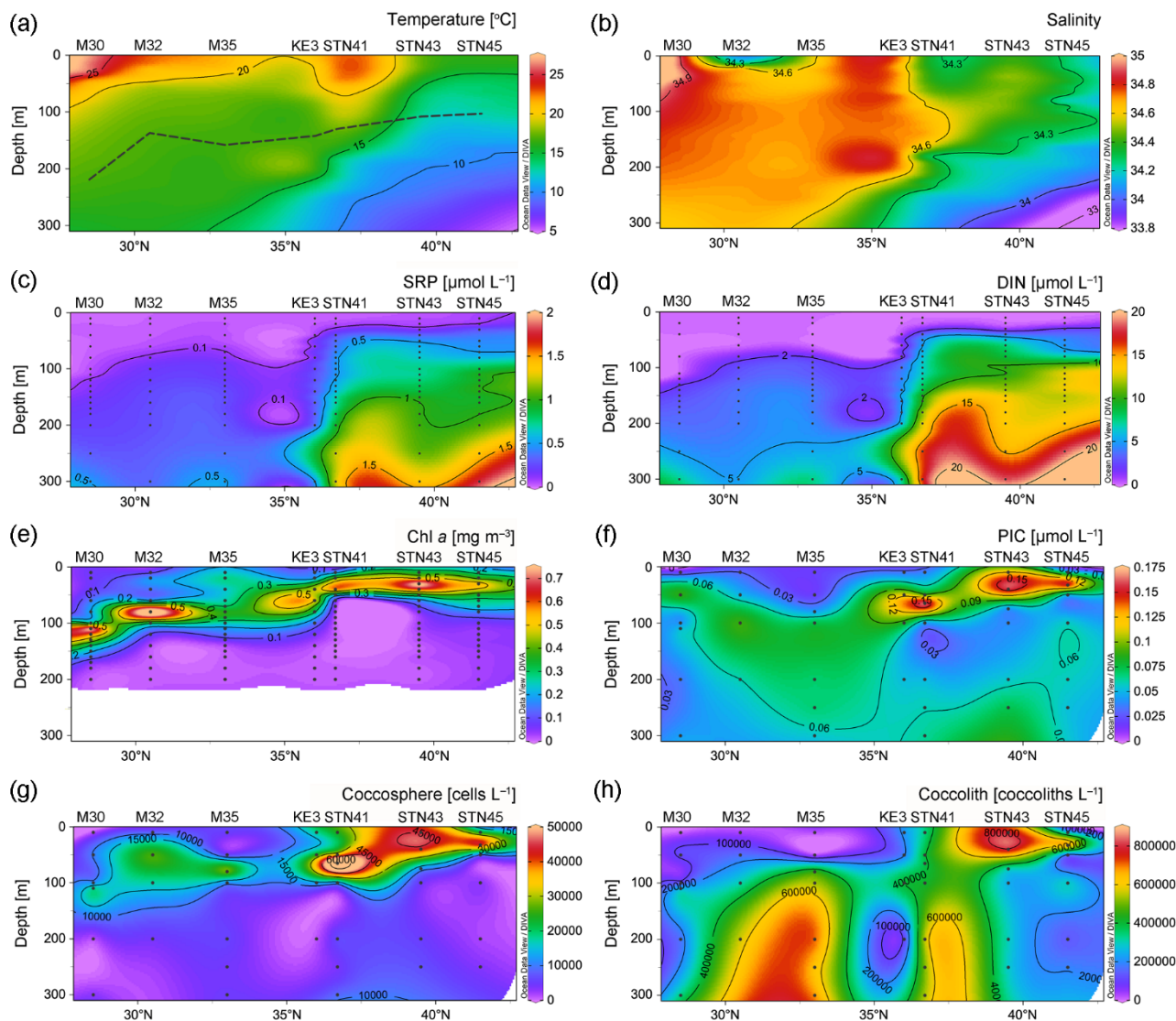


**Fig. 2.** Vertical depth distributions of (a) temperature, (b) salinity and concentrations of (c) soluble reactive phosphate (SRP), (d) dissolved inorganic nitrogen (DIN, nitrate plus nitrite), (e) Chlorophyll *a* (Chl *a*), (f) particulate inorganic carbon (PIC), (g) coccosphere cell and (h) detached coccoliths in the upper 300 m of the water column in the study area. In (a), the black dashed line indicates the bottom of the euphotic zone.

### 3.2 Vertical distribution of PIC and coccolithophore concentrations

PIC concentrations along the 155°E transect ranged from 0.02 to 0.17  $\mu\text{mol L}^{-1}$ , with an average of  $0.06 \pm 0.04 \mu\text{mol L}^{-1}$  in the upper 300 m of the water column (Fig. 2f). Generally, PIC concentrations were lower at the surface and increased with increasing depth to attain a maximum in the DCM layer, and decreased with depth thereafter. In the DCM layer, PIC concentrations ranged from 0.06  $\mu\text{mol L}^{-1}$  at 110 m of station M30 in the subtropical gyre to 0.16  $\mu\text{mol L}^{-1}$  at 33 m of station STN45 in the Kuroshio-Oyashio transition region. The vertical distribution pattern of bottle-derived PIC and coccosphere cell concentrations overall followed that of Chl *a*, showing a northward shoaling of the subsurface maximum.

Concentrations of coccosphere cells ranged from ca. 970 to 75,000 cells  $\text{L}^{-1}$  (Fig. 2g). Along the transect, a subsurface maximum was evidenced around the DCM layer with an average of 42,000 cells  $\text{L}^{-1}$ , followed by a steep decrease below 100 m. The highest coccosphere cell concentration was observed at 65 m of station STN41, corresponding to the highest PIC concentration. The average coccosphere cell concentration was notably lower in the NPSG region (9,800 cells  $\text{L}^{-1}$ ) than in the transition region (18,000 cells  $\text{L}^{-1}$ ). The detached coccolith concentration averaged 340,000 coccoliths  $\text{L}^{-1}$ , with a range of 11,000 to 800,000 coccoliths  $\text{L}^{-1}$  (Fig. 2h). The highest concentration was observed around 10–40 m of station STN43. High coccolith concentrations were also observed below 100 m at stations M32, M35 and STN41.

Size-fractionated PIC concentrations from in situ pumps varied from 0.01 to 0.09  $\mu\text{mol L}^{-1}$  in the small size fraction and from 0.01 to 0.06  $\mu\text{mol L}^{-1}$  in the large size fraction. Total PIC concentrations averaged  $0.07 \pm 0.02 \mu\text{mol L}^{-1}$ , and were comparable to bottle-derived PIC concentrations (Fig. 3). Roughly 70 % of the PIC was contributed by the small size fraction at each sampling station. Generally, large size fraction PIC concentrations increased northward from stations M30–M35 to stations KE3–STN45 and accounted for 22 % and 36 % of total PIC concentrations in the NPSG region and the Kuroshio-Oyashio transition region, respectively. The maximum concentration of large size-fractionated PIC (0.06  $\mu\text{mol L}^{-1}$ ) was observed at 26 m of station STN45 (Fig. 3g).

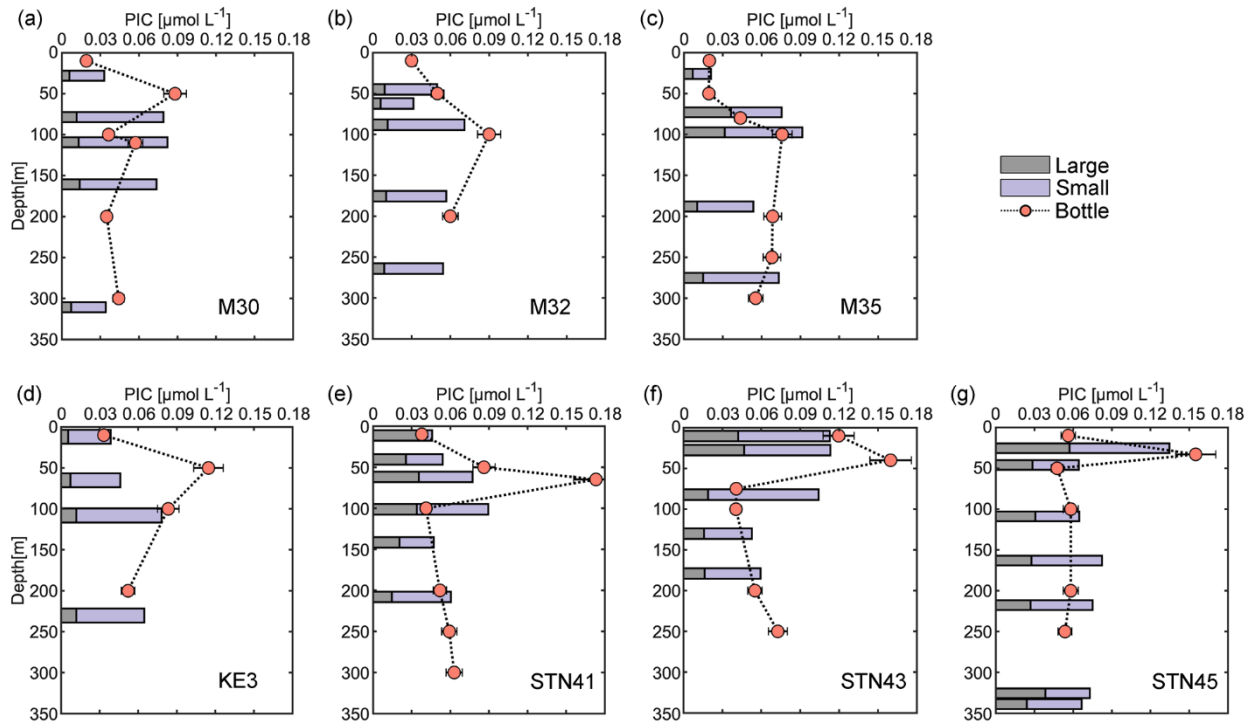
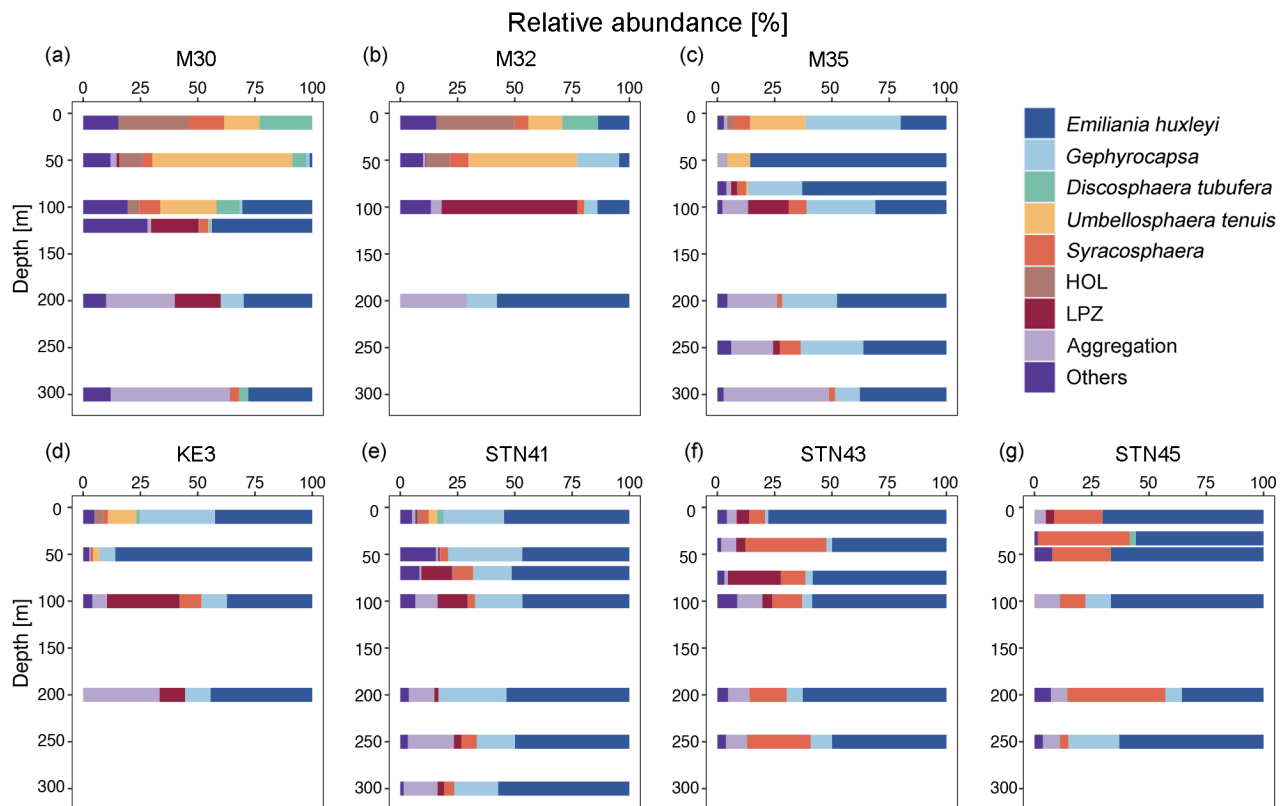


**Fig. 3.** Vertical depth distributions of particulate inorganic carbon (PIC) concentrations derived from sampling using both Niskin bottles and in situ pumps (small size fraction of 1–51  $\mu\text{m}$  and large size fraction of  $> 51 \mu\text{m}$ ) in the upper 350 m of the water column at sampling stations in the study area.

### 3.3 Characteristics of the coccolithophore assemblage

Coccolithophore populations were predominantly represented by *Emiliania huxleyi*, *Gephyrocapsa ericsonii*, *Gephyrocapsa oceanica*, *Umbellosphaera tenuis*, *Syracosphaera* spp., holo-coccolithophores (HOL), *Algirosphaera robusta*, and *Florisphaera profunda* (each comprising  $> 1\%$  of total coccosphere abundance; Fig. 4). In surface water, coccolithophore cells were dominated by *Discosphaera tubifera*, *U. tenuis* and HOL at stations M30 and M32 (Fig. 4a and b) and by *G. ericsonii* at stations M35, KE3 and STN41 (Fig. 4c, d and e), while high abundance of *E. huxleyi* and *Syracosphaera* spp. was clearly observed at stations STN43 and STN45 (Fig. 4f and g). It is noteworthy that *E. huxleyi* contributed the largest fraction (50 %) to the total coccolithophore cells and was also found to be the dominant species in the DCM layer. *U. tenuis* was mainly

238 observed in subtropical gyre waters, with peak abundance at 50 m and lower abundance at the surface and in the DCM (Fig.  
 239 4a and b). Lower euphotic zone (LPZ, defined as the region of the water column that receives 10–1% of surface PAR)  
 240 coccolithophore species (including *A. robusta* and *F. profunda*) were commonly found in the subsurface population below 50  
 241 m, accounting for 7 % of the entire coccolithophore community (Jin et al., 2016; Poulton et al., 2017). Overall,  
 242 coccolithophores were scarce in the NPSG region and dominated by *U. tenuis*, whereas their abundance notably increased in  
 243 the Kuroshio-Oyashio transition region where it was dominated by *E. huxleyi*, *Gephyrocapsa* and *Syracosphaera* spp..  
 244

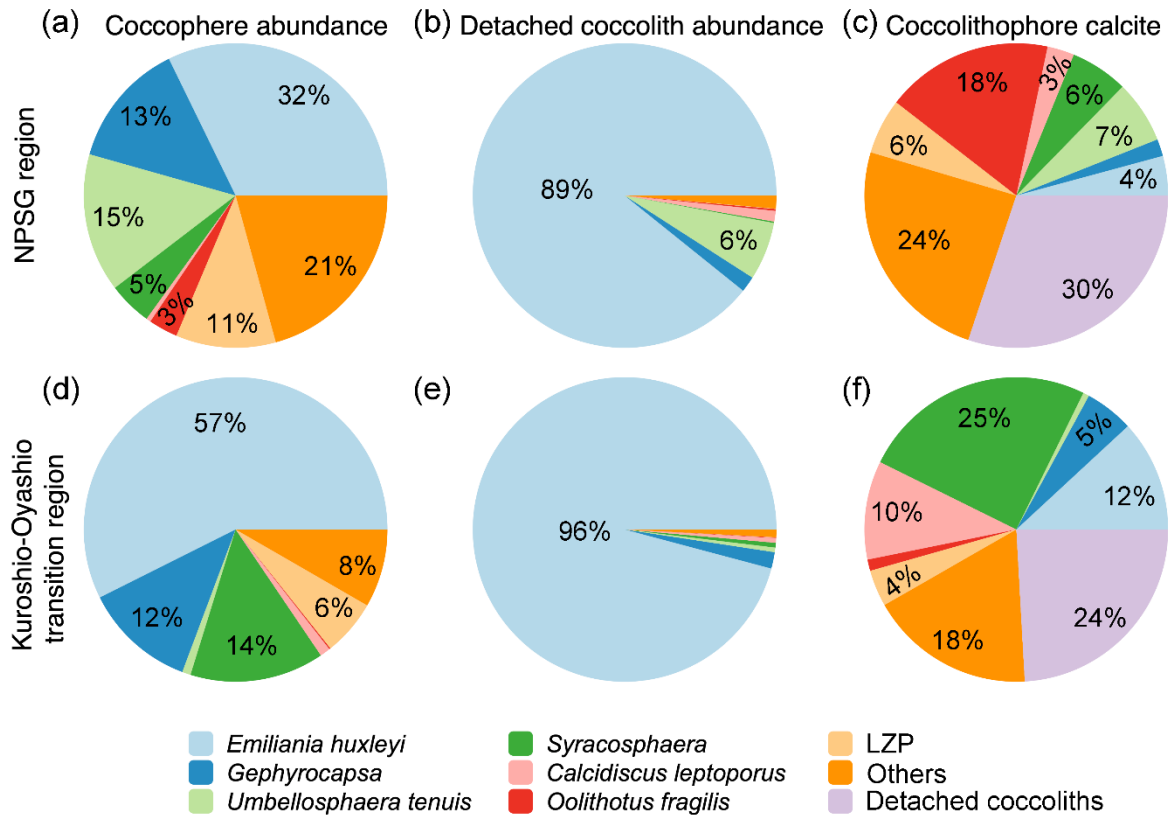


245  
 246 **Fig. 4.** Relative abundance of different coccolithophore groups in the upper 300 m of the water column. Lower euphotic zone  
 247 (LPZ) species include *Florisphaera profunda* and *Algirosphaera robusta*; HOL indicates holo-coccolithophores.

248

249 The estimated coccolithophore calcite concentrations ranged from  $<0.01$  to  $0.23 \mu\text{mol L}^{-1}$ , averaging  $0.05 \pm 0.04 \mu\text{mol L}^{-1}$

250 above 300 m along the 155°E transect. The coccospheres of *E. huxleyi* accounted for 32 % and 57 % of the total  
 251 coccolithophore cells but represented only 4 % and 12 % of the coccolithophore calcite concentration in the NPSG region and  
 252 the Kuroshio-Oyashio transition region, respectively (Fig. 5). In the NPSG region, *U. tenuis* accounted for 15 % of the total  
 253 coccolithophore cells and 7 % of the coccolithophore calcite concentration, both notably higher than in the transition region,  
 254 where its contribution was <1 % for both measures. *Syracosphaera* spp. was the largest contributor in the Kuroshio-Oyashio  
 255 transition region, accounting for 25 % of the coccolithophore calcite concentration (Fig. 5f). The less abundant (<3 %) species  
 256 *Calcidiscus leptoporus* and *Oolithotus fragilis* accounted for 21 % and 12 % of the coccolithophore calcite concentration in  
 257 the NPSG region and the Kuroshio-Oyashio transition region, respectively. Additionally, detached coccoliths contributed to  
 258 30 % and 24 % of the total coccolithophore calcite concentration in the two regions, respectively (Fig. 5c and f).  
 259



262 **Fig. 5.** Contribution of different coccolithophore groups to coccosphere cell abundance, detached coccolith abundance, and  
263 coccolithophore calcite concentrations in the upper 300 m of the water column in (a–c) the North Pacific Subtropical Gyre  
264 (NPSG, stations M30, M32 and M35) and (d–f) the Kuroshio-Oyashio transition region (stations KE3, STN41, STN43 and  
265 STN45). Lower euphotic zone (LPZ) species include *Florisphaera profunda* and *Algirosphaera robusta*.

266

### 267 **3.4 CaCO<sub>3</sub> standing stock and production**

268 The standing stocks of CaCO<sub>3</sub> in the euphotic zone were determined using data from Niskin bottles, coccolithophore calcite,  
269 and size-fractionated samples (Fig. 6a). CaCO<sub>3</sub> standing stock derived from Niskin bottle-sampling ranged from 7.0 to 11.1  
270 mmol m<sup>-2</sup>, and was slightly lower in the oligotrophic NPSG region ( $8.7 \pm 1.7$  mmol m<sup>-2</sup>) than in the relatively nutrient-high  
271 Kuroshio-Oyashio transition region ( $9.2 \pm 1.7$  mmol m<sup>-2</sup>). Based on the estimated coccolithophore calcite concentrations,  
272 CaCO<sub>3</sub> standing stocks ranged from 4.0 to 11.3 mmol m<sup>-2</sup> and peaked at station M30 due to its deepest euphotic zone (Fig. 2a  
273 and 6a). Calcite from coccolithophores comprised on average  $79 \pm 27$  % of the CaCO<sub>3</sub> standing stock from Niskin bottle  
274 samples, and the contribution was higher in the NPSG region ( $91 \pm 30$  %) than in the Kuroshio-Oyashio transition region ( $70$   
275  $\pm 24$  %; Fig. 6b), demonstrating the vital role of coccolithophores in CaCO<sub>3</sub> production, particularly in oligotrophic ocean  
276 waters.

277



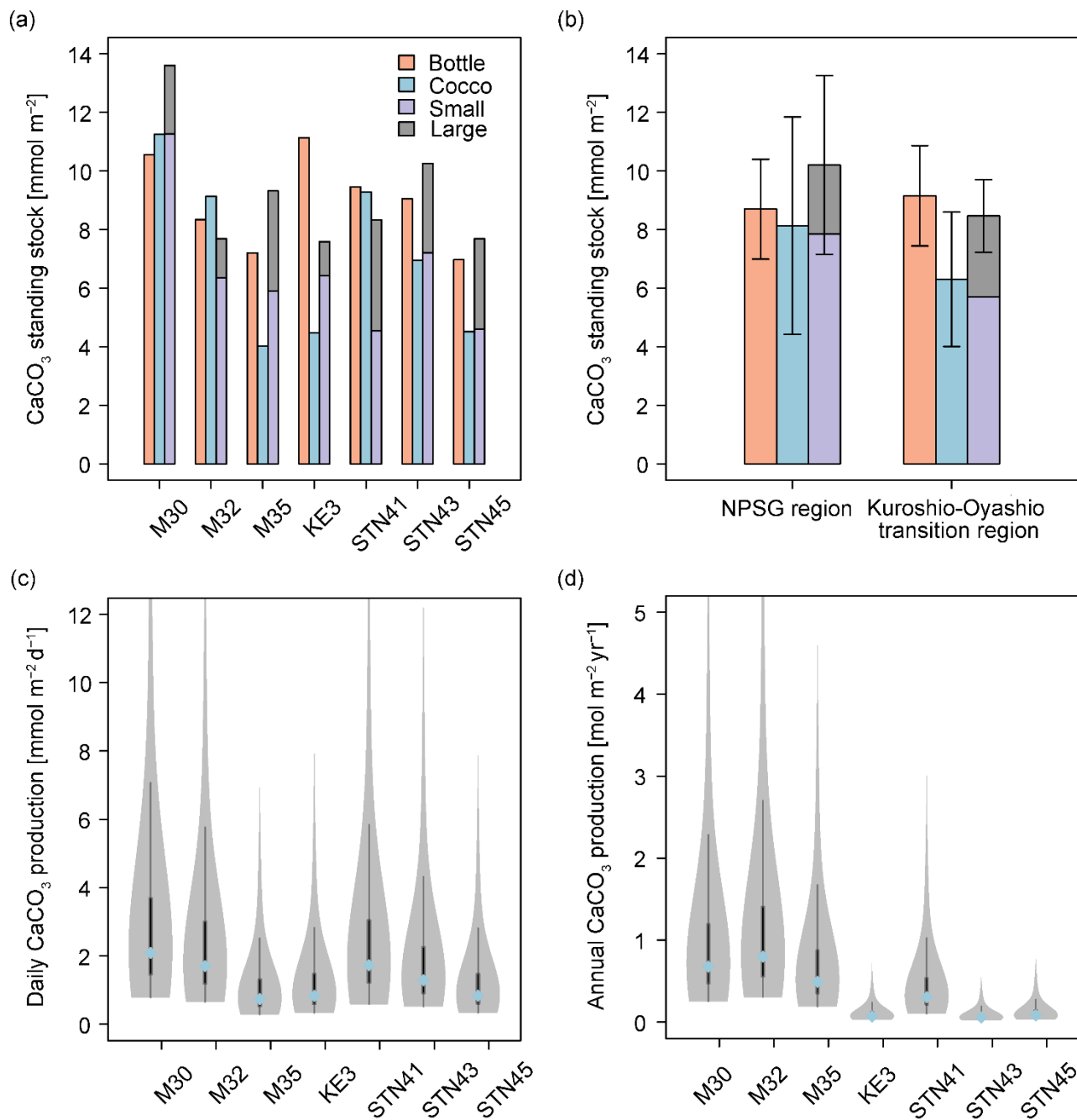


**Fig. 6.** Calcium carbonate (CaCO<sub>3</sub>) standing stock in the euphotic zone estimated from Niskin bottle particulate inorganic carbon (PIC), total calcite (Cocco) and size-fractionated (large and small fractions indicate > 51 and 1–51  $\mu$ m, respectively) PIC concentrations (a) at each sampling station and (b) in the North Pacific Subtropical Gyre (NPSG) and Kuroshio-Oyashio

282 transition regions; (c)  $\text{CaCO}_3$  production by coccolithophores in the euphotic zone at indicated sampling stations in June-July  
283 2022; (d) annual  $\text{CaCO}_3$  production corrected for seasonal bias using satellite-derived PIC concentrations. In (c) and (d), the  
284 blue diamond marks the median value, while the shaded area displays the probability density of the estimates. The grey lines  
285 denote the 25% and 75% quartiles.

286

287 Total  $\text{CaCO}_3$  standing stock derived from in situ pump samples ranged from 7.6 to 13.6  $\text{mmol m}^{-2}$ , averaging  $10.2 \pm 3.1$   
288  $\text{mmol m}^{-2}$  in the subtropical gyre and  $8.5 \pm 1.2 \text{ mmol m}^{-2}$  in the transition region. The  $\text{CaCO}_3$  standing stock of the small PIC  
289 ranged from 4.5 to 11.3  $\text{mmol m}^{-2}$  and accounted for  $71 \pm 12 \%$  of the total standing stock in the entire research domain (Fig.  
290 6a).

291 Given that coccolithophores have a turnover time of 0.7–10 days (Krumhardt et al., 2017; Ziveri et al., 2023),  $\text{CaCO}_3$   
292 production rate in the euphotic zone ranged from 0.8 to 2.1  $\text{mmol m}^{-2} \text{ d}^{-1}$  during the sampling period (Fig. 6c). Generally, the  
293 coccolithophore  $\text{CaCO}_3$  production was comparable in the subtropical gyre and the Kuroshio-Oyashio transition region,  
294 averaging  $1.5 \pm 0.7$  and  $1.2 \pm 0.4 \text{ mmol m}^{-2} \text{ d}^{-1}$ , respectively. Coccolithophore  $\text{CaCO}_3$  production in the euphotic zone was  
295 maximal at station M30 and the lowest coccolithophore  $\text{CaCO}_3$  production was observed at station M35.

296

## 297 **4 Discussion**

### 298 **4.1 Contribution of coccolithophore calcite to PIC**

299 In this study, bottle- and pump-derived PIC concentrations generally agreed with each other (Fig. 3), and both were on the  
300 same order of magnitude as suspended PIC concentrations measured in the Atlantic, Indian and Pacific Oceans (Beaufort et  
301 al., 2008; Barrett et al., 2014; Lam et al., 2015, 2018; Marañón et al., 2016). Coccolithophore calcite concentrations showed a  
302 significant positive correlation with PIC concentrations ( $r^2 = 0.52$ ,  $p < 0.01$ ,  $n = 40$ ; Fig. 7a), highlighting the major contribution  
303 of coccospheres and detached coccoliths (68 %) to total  $\text{CaCO}_3$  in the upper 300 m of the water column. This is consistent  
304 with findings from the eastern North Pacific Ocean where coccolithophores dominate  $\text{CaCO}_3$  production (Ziveri et al., 2023).  
305 It is noteworthy that detached coccolith concentrations of *E. huxleyi*, *U. tenuis* and *Syracosphaera* spp. showed a significant  
306 positive relationship with their coccosphere cell concentrations (Fig. 7b–d), indicating that those detached particles were likely

307 shed by cells as part of the dynamic calcification process, during which coccoliths are continuously produced and released  
308 (Johns et al., 2023). However, other potential sources and processes, such as advection, cell disintegration from viral lysis and  
309 grazing, fecal pellets, or the dissolution associated with microbial respiration could also contribute to the observed detached  
310 coccolith concentrations (Subhas et al., 2022; Vincent et al., 2023; Dean et al., 2024). Coccolith production and shedding vary  
311 among species. Fast-growing species like *E. huxleyi* produce and shed coccoliths rapidly during exponential growth phases,  
312 whereas other species exhibit different patterns, which are influenced by their distinct physiological and ecological  
313 characteristics (Johns et al., 2023).

314

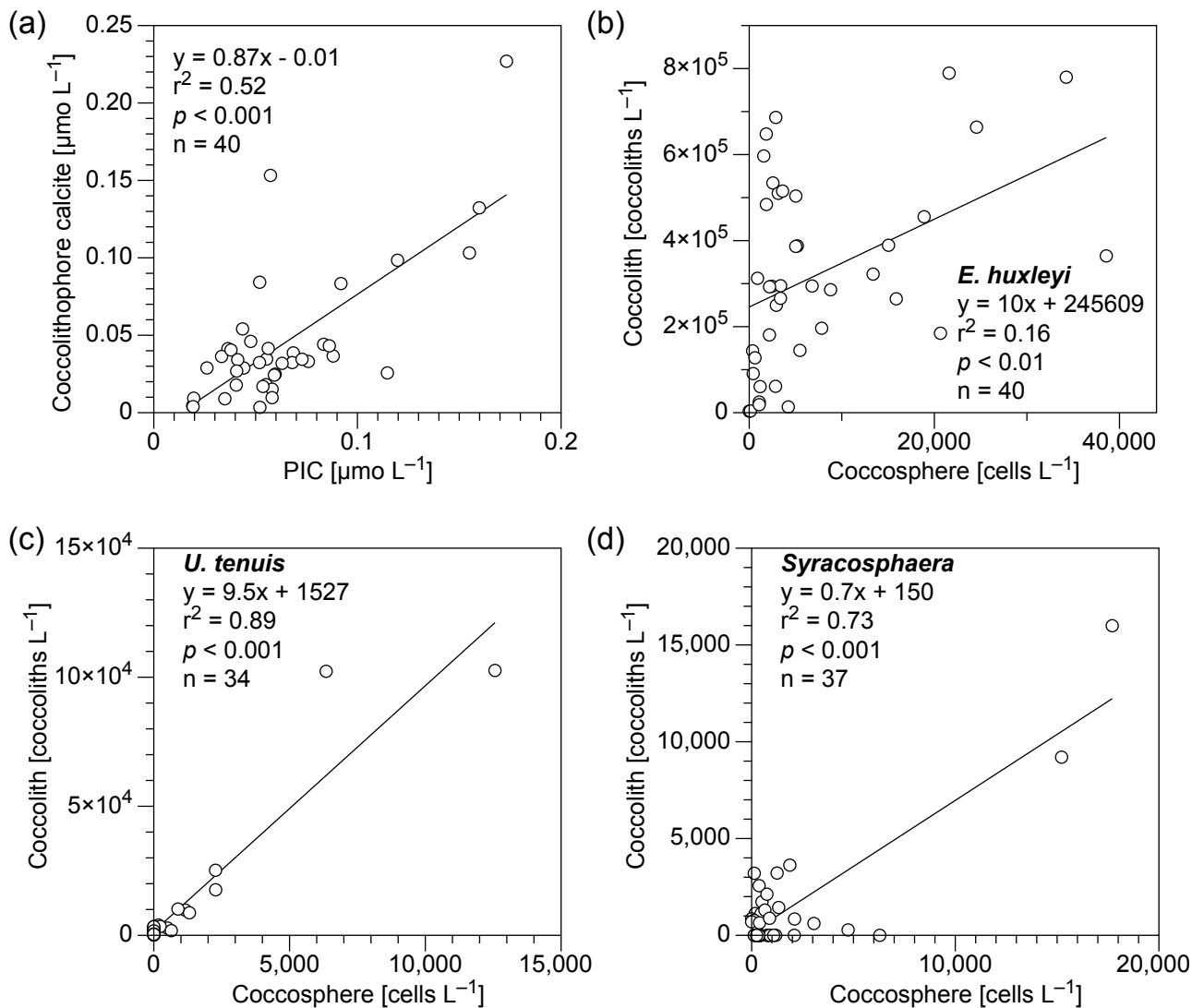


**Fig. 7.** Relationship of (a) coccolithophore calcite (coccospheres and detached coccoliths) vs particulate inorganic carbon (PIC) concentrations and (b–d) detached coccolith vs coccosphere cell concentrations for (b) *Emiliania huxleyi*, (c) *Umbellosphaera tenuis* and (d) *Syracosphaera* spp. in the upper 300 m water column in the study area. Equations describing the fitted straight lines are also shown.

The less abundant (<3 %) species such as *C. leptoporus* and *O. fragilis* also made a large contribution to calcite concentrations, accounting for 21 % and 12 % of the coccolithophore calcite concentration in the NPSG region and the

323 Kuroshio-Oyashio transition region, respectively (Fig. 5). It has been reported that despite the relatively low numeric  
324 abundance (<2 %), some larger species of the coccolithophore community such as *C. leptoporus*, *Helicosphaera carteri* and  
325 *Coccolithus pelagicus* may account for most of the coccolithophore CaCO<sub>3</sub> flux to the deep ocean (Rigual Hernández et al.,  
326 2020). Some rare coccolithophore species with high coccolith and coccosphere cell concentrations have also been identified  
327 as important contributors to both upper-ocean calcite production (Daniels et al., 2016) and deep-sea calcite fluxes (Ziveri et  
328 al., 2007). Thus, larger and less abundant coccolithophore species can play an important role in CaCO<sub>3</sub> production and export.

329 Higher CaCO<sub>3</sub> standing stock in the euphotic zone of the Kuroshio-Oyashio transition region (Fig. 6a) is consistent with  
330 satellite observations suggesting that higher surface PIC concentrations occur at high latitudes (Balch et al., 2005; Berelson et  
331 al., 2007). In the present study, however, the relative contribution of coccolithophores to the CaCO<sub>3</sub> standing stock was higher  
332 in the NPSG region (~91 %) than in the Kuroshio-Oyashio transition region (~70 %) (Fig. 6a). To date, most studies estimated  
333 CaCO<sub>3</sub> standing stocks using satellite-derived data, which might be challenging to use in subtropical gyres where the DCM  
334 depth usually lies below 100 m (Cornec et al., 2021). In these oligotrophic oceans with low productivity, a subsurface PIC  
335 maximum can develop within the euphotic zone, and the highly variable subsurface PIC concentrations are poorly reflected  
336 by satellites, potentially limiting the ability to fully capture coccolithophore contributions.

337 In oligotrophic ocean gyres, subsurface CaCO<sub>3</sub> production could still occur even if surface PIC is low (Balch et al., 2018).  
338 Along our studied transect, maximum coccolithophore abundances increased about twofold from the subtropical gyre to the  
339 transition region (Fig. 2g), while a much smaller difference was found in the integrated coccolithophore CaCO<sub>3</sub> between the  
340 two regions (Fig. 6a). This suggests that subsurface coccolithophore CaCO<sub>3</sub> contributed substantially to the total upper water  
341 column PIC concentration in the NPSG region. Coccolithophore groups were diverse in the subtropical gyre, including some  
342 rare but relatively large and heavily calcified species that contribute significantly to CaCO<sub>3</sub> production. In the Southern Ocean,  
343 coccolithophores contribution to the annual CaCO<sub>3</sub> export is highest in waters with low algal biomass accumulations (Rigual  
344 Hernández et al., 2020). Given that low surface PIC regions (<0.1 mmol m<sup>-3</sup>) occupy about 87 % of the global ocean surface  
345 (Ziveri et al., 2023), our data highlight the notable contribution of these regions to global coccolithophore CaCO<sub>3</sub> production.

346 Size-fractionated PIC concentrations showed a smaller contribution of coccolithophores to the CaCO<sub>3</sub> standing stock in the  
347 Kuroshio-Oyashio transition region (67 ± 13 %) than in the NPSG region (76 ± 11 %) (Fig. 6b). This pattern is consistent with

348 that observed in the eastern North Pacific Ocean (Fig. 8), which suggests that the contribution of small PIC to  $\text{CaCO}_3$  standing  
349 stock is lower in the subpolar gyre (65 %) than in the subtropical gyre (84 %). In other words, the contribution of large size  
350 fraction PIC (e.g., zooplanktonic foraminifera, pteropods and heteropods) to  $\text{CaCO}_3$  standing stock is higher in the subpolar  
351 gyre (35 %) than in the subtropical gyre (16 %) of the eastern North Pacific Ocean (Ziveri et al., 2023). Betzer et al. (1984)  
352 reported that foraminifera calcite is more abundant in northern regions (north of  $42^\circ\text{N}$ ) of the western North Pacific. At Ocean  
353 Station Papa in the northeast Pacific ( $50^\circ\text{N}$ ,  $145^\circ\text{W}$ ), model results showed that foraminifera calcite accounts for only 18–30 %  
354 of the total  $\text{CaCO}_3$  production, whereas coccolithophores are the main producer, contributing to 59–77 % of the total  $\text{CaCO}_3$   
355 production (Fabry, 1989). These findings support our results and suggest that the relatively high contribution of large size  
356 fraction PIC in the northern region of the western North Pacific is likely attributed to foraminifera.

357 In the Atlantic Ocean, coccolithophore calcite fluxes and species richness are higher in subtropical than in temperate waters,  
358 which is ascribed to the reduced competition with diatoms in the former (Broerse et al., 2000). Note that a clear latitudinal  
359 gradient of diatom biomass was observed along  $160^\circ\text{E}$  in the North Pacific Ocean, consistent with findings from phytoplankton  
360 pigment analysis and ocean-color satellite observations (Hirata et al., 2011; Sugie and Suzuki, 2017). The distribution of  
361 planktic foraminifera in the North Pacific has been linked to phytoplankton productivity and food availability, with higher  
362 abundance in the transitional region compared to the subtropical region (Taylor et al., 2018). Based on these findings, we  
363 suggest that differences in ecosystem structure among sites modulate the relative contribution of various calcifiers to pelagic  
364 PIC production. The higher abundance of non-calcareous phytoplankton (e.g., diatoms) in the transition zone could also reduce  
365 coccolithophore biomass via resource competition (Quere et al., 2005; Sinha et al., 2010) and stimulate the growth of  
366 foraminifera (Schiebel et al., 2017), resulting in the observed decreased contribution of small coccolithophores to total  $\text{CaCO}_3$   
367 production. Sediment trap data from the North Pacific also support this pattern, indicating lower fluxes of planktonic  
368 foraminifera, organic matter, and biogenic opal in the subtropical region but elevated fluxes in the transitional and subarctic  
369 regions (Eguchi et al., 2003).

370

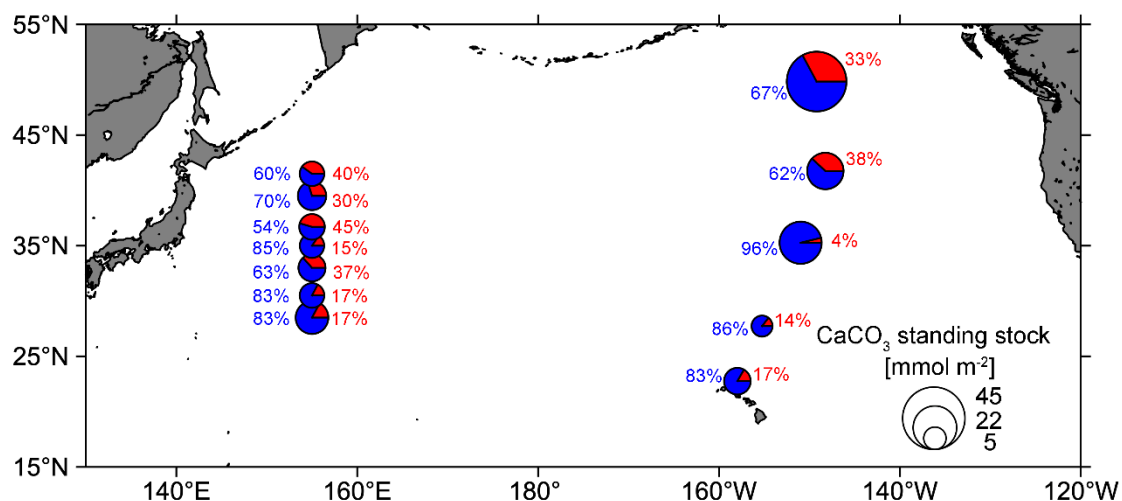


**Fig. 8.** Pie charts showing the composition of the total calcium carbonate (CaCO<sub>3</sub>) standing stock in the euphotic zone of the western (this study) and eastern North Pacific Ocean (data from the CDisK-IV cruise; Ziveri et al., 2023). Red represents the standing stock of large size-fractionated (> 51 μm) CaCO<sub>3</sub> from this study, and planktonic foraminifera, pteropods and heteropods from the CDisK-IV cruise. Blue represents the standing stock of small size-fractionated (1–51 μm) CaCO<sub>3</sub> from this study and coccolithophores from the CDisK-IV cruise.

## 4.2 Coccolithophore responses to environmental factors

Although biogeographical zones of coccolithophores in the North and Central Pacific were identified a couple of decades ago, few studies have investigated coccolithophore distributions in the North Pacific over the recent two decades (Okada and Honjo, 1973; Hagino et al., 2005). In the western North Pacific Ocean, higher diversity and less abundant coccolithophore assemblages were observed in the oligotrophic subtropical gyres, whereas the Kuroshio-Oyashio transition region tended to exhibit a lower diversity corresponding to higher PIC and coccolithophore concentrations (Figs. 2 and S2). This finding is consistent with results from the Atlantic Ocean, and a result of the different survival strategies of various coccolithophore species (Poulton et al., 2017; Balch et al., 2019). Coccolithophores are nutrient stress tolerant and have low iron cell quotas, thus generally abundant in the open ocean (Gregg and Casey, 2007; Brun et al., 2015). Prior studies have shown that coccolithophores, particularly *E. huxleyi*, can grow more effectively under low iron conditions than other phytoplankton such as diatoms (Hartnett

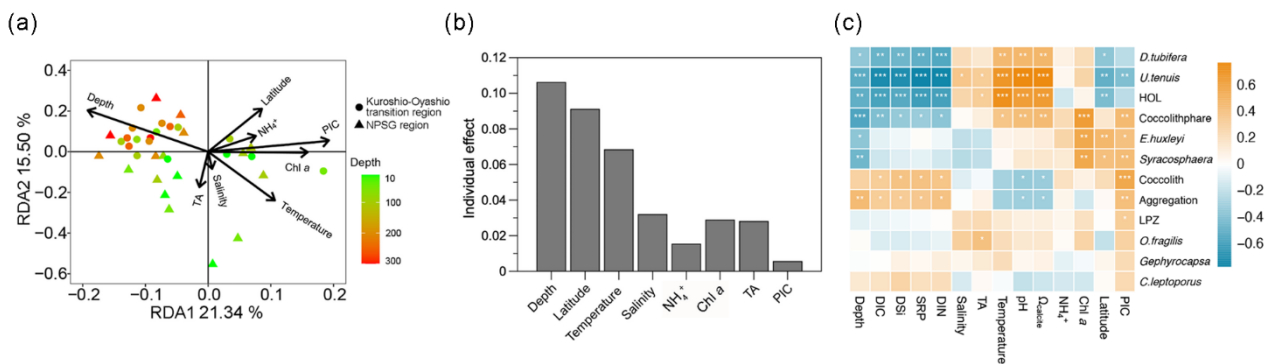
et al., 2012; Balch, 2018). However, when nutrients and light are plentiful, the heavy coccoliths of this group of phytoplankters pose a selective disadvantage over diatoms and chlorophytes (Gregg and Casey, 2007). The dominance of coccolithophores in the Great Calcite Belt is primarily driven by their adaptation to low iron levels, which, together with low surface  $DSi$  concentrations, limit diatom growth (Balch et al., 2016). The majority of coccolithophore species are K-selected, characterized by relatively slow-growth, large cell size and are more competitive in low-nutrient and well-stratified regions (Brand, 1994), whereas only few r-selected species, such as the fast-growing and small-sized *E. huxleyi* thrive in relatively dynamic and nutrient-rich regions (Charalampopoulou, 2011; Brun et al., 2015; O'Brien et al., 2016). In the present study, the most abundant and widely distributed coccolithophore species was *E. huxleyi*, which showed increasing abundance northward along the study transect (Fig. 4). This is consistent with prior observations demonstrating that *E. huxleyi* is the most abundant coccolithophore species in the subarctic, subantarctic and bordering transitional regions (Saavedra-Pellitero et al., 2014).

According to the RDA results, environmental variables accounted for 47.6 % of the total variation in coccolithophore community composition (Fig. 9a). The first two RDA axes suggested that there were significant spatial differences in the coccolithophore community across depths and regions (Fig. S3). In the tropical and subtropical Atlantic Ocean, coccolithophore communities exhibit greater variability vertically within the water column than horizontally, at spatial scales of hundreds to thousands of kilometers (Poulton et al., 2017). Moreover, distinct species distributions are identified based on the depth zones (upper euphotic, lower euphotic, and subeuphotic zones), which reflect the lifestyle of the species (Poulton et al., 2017; Balch, 2018). In the NPSG region, our results also reveal a distinct vertical distribution pattern (Fig. 4), which may have been driven by factors such as light availability, temperature, and nutrient levels. These environmental variables likely contribute to the physiological diversity of coccolithophores. A shift in dominant species occurred from *U. tenuis* and *E. huxleyi* in the NPSG region to *Syracosphaera* spp. and *E. huxleyi* in the transition region (Fig. 5). This is consistent with the prior observations of Balch et al. (2019). Correspondingly, hierarchical partitioning analysis showed that depth and latitude had a significant effect on coccolithophore community variation ( $p < 0.05$ ). Other environmental factors, such as temperature, salinity, Chl *a* and TA also influenced the coccolithophore community (Fig. 9b).

Based on Spearman's correlation analysis, coccolithophore abundance showed a significant positive relationship with temperature,  $\Omega_{calcite}$  and pH, and a significant negative relationship with depth, DIC and macro-nutrient concentrations,



413 especially for *D. tubifera*, *U. tenuis* and HOL that are more sensitive to environmental factors (Fig. 9c). The positive correlation  
 414 with temperature is consistent with field observations and model simulations pointing to a general trend of increasing  
 415 coccolithophore abundance in the context of global warming (Rivero-Calle et al., 2015; Rousseaux and Gregg, 2015). More  
 416 abundant species like *E. huxleyi* and *Syracosphaera* spp., however, only showed a highly positive correlation with depth,  
 417 latitude and Chl *a* concentration, suggesting that these species are more adaptable to varying environmental conditions  
 418 (Schlüter et al., 2014). In the Atlantic Ocean, *E. huxleyi* has been observed to exhibit an increasing relative abundance with  
 419 increasing latitude (Balch et al., 2019; Holligan et al., 2010; Poulton et al., 2017). Unlike many other species, *E. huxleyi* has a  
 420 widespread distribution attributed to its ability to adapt to diverse environments through both phenotypic plasticity and genetic  
 421 selection (Lohbeck et al., 2012; Rickaby et al., 2016b; Taylor et al., 2017). Our results indicate that less abundant species, such  
 422 as *C. leptoporus* and *O. fragilis*, also contributed to coccolithophore calcite concentrations (Fig. 5). Their calcification is  
 423 species-specific, predominantly driven by inherent biological traits, including cell shapes, coccolith types, and architectural  
 424 variations, which are conservative features of coccolithophore biology (Rickaby et al., 2016a). However, the weak correlation  
 425 of *C. leptoporus* and *O. fragilis* with environmental factors might be due to their low abundance. Overall, our study highlights  
 426 the significant influence of depths and latitude on coccolithophore community composition, emphasizing the complex interplay  
 427 between biotic and abiotic factors.  
 428



429  
 430 **Fig. 9.** (a) Redundancy analysis (RDA) diagram illustrating the relationship between the coccolithophore community and  
 431 environmental factors; (b) independent contribution of each environmental factor to coccolithophore community variation

432 using hierarchical partitioning-based canonical analysis; (c) correlations between coccolithophore groups and environmental  
433 factors with color gradients denoting the significance of the Spearman's correlation coefficient  $r$ . Asterisks represent the  
434 statistical significance ( $***p < 0.001$ ,  $**p < 0.01$ ,  $*p < 0.05$ ). Chl  $a$ : chlorophyll  $a$ , DIC: dissolved inorganic carbon, TA: total  
435 alkalinity,  $\Omega_{\text{calcite}}$ : saturation state with respect to calcite, PIC: particulate inorganic carbon, DIN: dissolved inorganic nitrogen  
436 (nitrate plus nitrite),  $\text{NH}_4^+$ : ammonium, SRP: soluble reactive phosphate, DSi: dissolved silicate, HOL: holo-coccolithophores  
437 and LPZ: lower euphotic zone species *Florisphaera profunda* and *Algirosphaera robusta*.

### 438 439 **4.3 CaCO<sub>3</sub> production compared with the eastern North Pacific**

440 While  $^{14}\text{C}$  incubations can provide a direct and precise measurement of in situ calcification rates, the calculation method we  
441 used offers a practical approach to convert concentration data into production estimates using turnover time (Graziano et al.,  
442 2000; Ziveri et al., 2023). This approach has limitations, particularly due to uncertainties in the estimation of coccolithophore  
443 calcite, which relies on cell counts and a morphometric-based calcite estimation method, with potential errors reaching up to  
444 50% (Young and Ziveri, 2000; Sheward et al., 2024). The calculation of production rates introduces further uncertainty, as it  
445 depends on the coccolithophore calcite standing stock and a broad range of turnover time estimates. Despite these challenges,  
446 this method produces reasonable results that are comparable to field observations and thus helps fill a critical data gap in the  
447 study region.

448 Our results indicate that the coccolithophore  $\text{CaCO}_3$  production ranged from 0.8 to 2.1  $\text{mmol m}^{-2} \text{d}^{-1}$  during the sampling  
449 period, align with globally reported in situ calcification rates and are consistent with observations from the North Atlantic  
450 subtropical region (Poulton et al., 2006; Daniels et al., 2018). Although station M30 is located in the oligotrophic NPSG region,  
451 it exhibits the highest coccolithophore  $\text{CaCO}_3$  production in the euphotic zone of the study area (Fig. 6c). This is primarily  
452 because of the deepest euphotic zone at this site, reaching up to 219 m, and the relatively high coccolithophore species diversity.  
453 While the coccolithophore abundance at station M30 was lower than at other stations, the less abundant but larger species play  
454 an important role in contributing to the  $\text{CaCO}_3$  production at this site.

455 Using a seasonal-correction method (Ziveri et al., 2023), the average coccolithophore  $\text{CaCO}_3$  production in the euphotic  
456 zone was estimated to be  $0.4 \pm 0.3 \text{ mol m}^{-2} \text{yr}^{-1}$  for the entire research domain. In particular, this production was  $0.66 \pm 0.2$

457 mol m<sup>-2</sup> yr<sup>-1</sup> in the subtropical gyre and 0.13 ± 0.1 mol m<sup>-2</sup> yr<sup>-1</sup> in the Kuroshio-Oyashio transition region (Fig. 6d). However,  
458 the latter is much lower than the recent estimate of 0.9–1.0 mol m<sup>-2</sup> yr<sup>-1</sup> by Ziveri et al. (2023) based on data from the transition  
459 zone and subpolar gyre in the eastern North Pacific Ocean using the same seasonal-correction method.

460 Several factors may lead to the above discrepancy. First, CaCO<sub>3</sub> production rate on the present study was estimated based  
461 only on coccolithophores, whereas estimates by Ziveri et al. (2023) also included the contribution from planktonic foraminifera,  
462 pteropods and heteropods. Second, in the CDisK-IV cruise to the eastern North Pacific Ocean, coccolithophore calcite  
463 concentrations were significantly higher than suspended seawater PIC concentrations collected by in situ pumps in the  
464 transition zone and subpolar gyre (Fig. S4; Dong et al., 2019, 2022). Calculations based on these apparently inconsistent data  
465 may result in an overestimation of actual CaCO<sub>3</sub> production. Third, high spatial and seasonal variations in PIC production  
466 might occur between the two oceanic environments. Particularly, the complex environmental gradients and variability in the  
467 transition regions between the subtropical and subpolar gyres may have skewed the coccolithophore community and associated  
468 CaCO<sub>3</sub> production.

469 Overall, our findings suggest that while satellite-derived PIC can reflect surface-layer distribution patterns, its calibration  
470 should be interpreted with caution, as it does not reliably capture total water column PIC production. We observed a significant  
471 positive relationship between surface coccolithophore calcite concentrations and satellite-derived PIC concentrations ( $r^2 = 0.84$ ;  
472  $p < 0.01$ ; Fig. S5a), indicating that satellite data can reflect the spatial distribution trends of the surface calcite. However, this  
473 correlation does not extend to actual values, particularly in high latitude areas where satellite-derived PIC is likely  
474 overestimated. Across the full euphotic zone, no significant correlation was found between satellite-derived PIC and measured  
475 PIC production, which is also noted by Ziveri et al. (2023) for the CDisK-IV cruise (Fig. S5b). More in situ measurements,  
476 such as calcification rates determined from <sup>14</sup>C incubations and direct measurements of coccolithophore turnover time, are  
477 needed to reduce uncertainties in estimating PIC production and assessing the oceanic CaCO<sub>3</sub> budget.

478

## 479 5 Conclusions

480 We have demonstrated that coccolithophore abundance and species composition had distinct geographic and vertical  
481 distribution patterns, with *U. tenuis* dominating in the NPSG region while *E. huxleyi* and *Syracosphaera* spp. in the Kuroshio-

482 Oyashio transition region. The environmental variables that best described varying coccolithophore communities were depth  
483 and latitude. Calcite derived from coccolithophores contributed  $79 \pm 27$  % of the PIC standing stocks in the euphotic zone,  
484 with a relatively greater contribution in the subtropical gyre than in the transition region. Less abundant ( $<3$  %) species such  
485 as *C. leptoporus* and *O. fragilis* also made a large contribution of 21 % and 12 % to the coccolithophore calcite concentration  
486 in the NPSG region and the Kuroshio-Oyashio transition region, respectively. During the sampling period, coccolithophore  
487  $\text{CaCO}_3$  production ranged from 0.8 to 2.1  $\text{mmol m}^{-2} \text{d}^{-1}$  in the entire research domain, averaging  $1.5 \pm 0.7$   $\text{mmol m}^{-2} \text{d}^{-1}$  in the  
488 subtropical gyre and  $1.2 \pm 0.4$   $\text{mmol m}^{-2} \text{d}^{-1}$  in the Kuroshio-Oyashio transition region. Given the important role of  $\text{CaCO}_3$   
489 dynamics in the marine alkalinity and carbon cycles, coccolithophore production at different scales from seasonal to annual  
490 and from regional to global needs further examination.

491 *Data availability.* Data for temperature, salinity, coccolithophore cell and coccolith abundances, coccolithophore calcite, PIC  
492 and nutrients concentrations can be downloaded from the Science Data Bank (<https://www.scidb.cn/en/s/i6bMFn>). Satellite-  
493 based temperature, Chl *a* and PIC concentration data were obtained from the MODIS-Aqua satellite  
494 (<https://oceancolor.gsfc.nasa.gov/l3/>).

495  
496 *Supplement link.*

497  
498 *Author Contributions.* YH, ZC, and MD conceived and designed the study. YH, ZS, DF, and JC contributed to data acquisition  
499 and analysis. YH, ZS, ZC, and MD wrote the first draft of the manuscript. YH, ZS, ZC, JY, and MD discussed results and  
500 edited the paper. All authors read and approved the final version of the manuscript.

501  
502 *Competing interests.* The authors declare that they have no conflict of interests.

503  
504 *Disclaimer.*

505  
506 *Acknowledgements.* The captain and the crew of R/V *Tan Kah Kee* are acknowledged for their cooperation during the cruise.  
507 We thank Feipeng Xu and Xin Liu for providing the chlorophyll *a* data, Lifang Wang, Tao Huang, Yanmin Wang and Zhijie  
508 Tan for the nutrient data, Yi Yang and Xianghui Guo for the carbonate system data, Xuchen Wang for advice on particulate  
509 inorganic carbon measurements, and Yanping Xu for logistical assistance. Yuye Han was supported by the Joint Training  
510 Program in Marine Environmental Sciences sponsored by the China Scholarship Council. Constructive comments by Alex  
511 Poulton, Chloe Dean, and Olivier Sulpis greatly improved the quality of this contribution.

512  
513 *Financial support.* This research was funded by the National Natural Science Foundation of China (NSFC project No.  
514 42141003 and 42188102). Data and samples were collected onboard the R/V *Tan Kah Kee* implementing the open research  
515 cruise NORC2022-306 supported by NSFC Shiptime Sharing Project (project No. 42149303).

516 **References**

- 517 Armstrong, R. A., Lee, C., Hedges, J. I., Honjo, S., and Wakeham, S. G.: A new, mechanistic model for organic carbon fluxes  
518 in the ocean based on the quantitative association of POC with ballast minerals, *Deep sea research II*, 49, 219-236,  
519 [https://doi.org/10.1016/S0967-0645\(01\)00101-1](https://doi.org/10.1016/S0967-0645(01)00101-1), 2001.
- 520 Balch, W., Drapeau, D., Bowler, B., and Booth, E.: Prediction of pelagic calcification rates using satellite measurements, *Deep*  
521 *sea research II*, 54, 478-495, <https://doi.org/10.1016/j.dsr2.2006.12.006>, 2007.
- 522 Balch, W., Gordon, H. R., Bowler, B., Drapeau, D., and Booth, E.: Calcium carbonate measurements in the surface global  
523 ocean based on Moderate-Resolution Imaging Spectroradiometer data, *J Geophys Res-Oceans*, 110,  
524 <https://doi.org/10.1029/2004jc002560>, 2005.
- 525 Balch, W. M.: The ecology, biogeochemistry, and optical properties of coccolithophores, *Annu Rev Mar Sci*, 10, 71-98,  
526 <https://doi.org/10.1146/annurev-marine-121916-063319>, 2018.
- 527 Balch, W. M., Bowler, B. C., Drapeau, D. T., Lubelczyk, L. C., and Lyczkowski, E.: Vertical distributions of coccolithophores,  
528 PIC, POC, biogenic Silica, and chlorophyll a throughout the global ocean, *Global Biogeochem Cy*, 32, 2-17,  
529 <https://doi.org/10.1002/2016gb005614>, 2018.
- 530 Balch, W. M., Bowler, B. C., Drapeau, D. T., Lubelczyk, L. C., Lyczkowski, E., Mitchell, C., and Wyeth, A.: Coccolithophore  
531 distributions of the north and south Atlantic ocean, *Deep sea research I*, 151, 103066, <https://doi.org/10.1016/j.dsr.2019.06.012>,  
532 2019.
- 533 Balch, W. M., Bates, N. R., Lam, P. J., Twining, B. S., Rosengard, S. Z., Bowler, B. C., Drapeau, D. T., Garley, R., Lubelczyk,  
534 L. C., and Mitchell, C.: Factors regulating the Great Calcite Belt in the Southern Ocean and its biogeochemical significance,  
535 *Global Biogeochem Cy*, 30, 1124-1144, <https://doi.org/10.1002/2016GB005414>, 2016.
- 536 Barrett, P. M., Resing, J. A., Buck, N. J., Feely, R. A., Bullister, J. L., Buck, C. S., and Landing, W. M.: Calcium carbonate  
537 dissolution in the upper 1000 m of the eastern North Atlantic, *Global Biogeochem Cy*, 28, 386-397,  
538 <https://doi.org/10.1002/2013gb004619>, 2014.
- 539 Beaufort, L., Couapel, M., Buchet, N., Claustre, H., and Goyet, C.: Calcite production by coccolithophores in the south east  
540 Pacific Ocean, *Biogeosciences*, 5, 1101-1117, <https://doi.org/10.5194/bg-5-1101-2008>, 2008.

541 Berelson, W., Balch, W., Najjar, R., Feely, R., Sabine, C., and Lee, K.: Relating estimates of CaCO<sub>3</sub> production, export, and  
 542 dissolution in the water column to measurements of CaCO<sub>3</sub> rain into sediment traps and dissolution on the sea floor: A revised  
 543 global carbonate budget, *Global Biogeochem Cy*, 21, <https://doi.org/10.1029/2006gb002803>, 2007.

544 Betzer, P., Byrne, R., Acker, J., Lewis, C., Jolley, R., and Feely, R.: The oceanic carbonate system: a reassessment of biogenic  
 545 controls, *Science*, 226, 1074-1077, <https://doi.org/10.1126/science.226.4678.1074>, 1984.

546 Boeckel, B. and Baumann, K.-H.: Vertical and lateral variations in coccolithophore community structure across the subtropical  
 547 frontal zone in the South Atlantic Ocean, *Mar Micropaleontol*, 67, 255-273, <https://doi.org/10.1016/j.marmicro.2008.01.014>,  
 548 2008.

549 Bollmann, J., Cortés, M. Y., Haidar, A. T., Brabec, B., Close, A., Hofmann, R., Palma, S., Tupas, L., and Thierstein, H. R.:  
 550 Techniques for quantitative analyses of calcareous marine phytoplankton, *Mar Micropaleontol*, 44, 163-185,  
 551 [https://doi.org/10.1016/s0377-8398\(01\)00040-8](https://doi.org/10.1016/s0377-8398(01)00040-8), 2002.

552 Brand, L.: Physiological ecology of marine coccolithophores, *Coccolithophores*, 39-50 pp.1994.

553 Broecker, W. S. and Peng, T.-H.: Tracers in the Sea, Lamont-Doherty Geological Observatory, Columbia University Palisades,  
 554 New York, 1982.

555 Broerse, A. T., Ziveri, P., van Hinte, J. E., and Honjo, S.: Coccolithophore export production, species composition, and  
 556 coccolith-CaCO<sub>3</sub> fluxes in the NE Atlantic (34°N 21°W and 48°N 21°W), *Deep sea research II*, 47, 1877-1905,  
 557 [https://doi.org/10.1016/s0967-0645\(00\)00010-2](https://doi.org/10.1016/s0967-0645(00)00010-2), 2000.

558 Brun, P., Vogt, M., Payne, M. R., Gruber, N., O'Brien, C. J., Buitenhuis, E. T., Le Quéré, C., Leblanc, K., and Luo, Y. W.:  
 559 Ecological niches of open ocean phytoplankton taxa, *Limnol Oceanogr*, 60, 1020-1038, <https://doi.org/10.1002/lno.10074>,  
 560 2015.

561 Cai, W.-J., Dai, M., Wang, Y., Zhai, W., Huang, T., Chen, S., Zhang, F., Chen, Z., and Wang, Z.: The biogeochemistry of  
 562 inorganic carbon and nutrients in the Pearl River estuary and the adjacent Northern South China Sea, *Cont Shelf Res*, 24, 1301-  
 563 1319, <https://doi.org/10.1016/j.csr.2004.04.005>, 2004.

564 Cai, W. J., Hu, X., Huang, W. J., Jiang, L. Q., Wang, Y., Peng, T. H., and Zhang, X.: Alkalinity distribution in the western North  
 565 Atlantic Ocean margins, *J Geophys Res-Oceans*, 115, <https://doi.org/10.1029/2009jc005482>, 2010.

Charalampopoulou, A.: Coccolithophores in high latitude and polar regions: relationships between community composition, calcification and environmental factors, University of Southampton, 2011.

Cornec, M., Laxenaire, R., Speich, S., and Claustre, H.: Impact of mesoscale eddies on deep chlorophyll maxima, *Geophys Res Lett*, 48, e2021GL093470, <https://doi.org/10.1029/2021GL093470>, 2021.

Daniels, C. J., Poulton, A. J., Young, J. R., Esposito, M., Humphreys, M. P., Ribas-Ribas, M., Tynan, E., and Tyrrell, T.: Species-specific calcite production reveals *Coccolithus pelagicus* as the key calcifier in the Arctic Ocean, *Mar Ecol Prog Ser*, 555, 29-47, <https://doi.org/10.3354/meps1182>, 2016.

Daniels, C. J., Poulton, A. J., Balch, W. M., Marañón, E., Adey, T., Bowler, B. C., Cermeño, P., Charalampopoulou, A., Crawford, D. W., and Drapeau, D.: A global compilation of coccolithophore calcification rates, *Earth Syst Sci Data*, 10, 1859-1876, <https://doi.org/10.5194/essd-10-1859-2018>, 2018.

Dean, C. L., Harvey, E. L., Johnson, M. D., and Subhas, A. V.: Microzooplankton grazing on the coccolithophore *Emiliana huxleyi* and its role in the global calcium carbonate cycle, *Science Advances*, 10, eadr5453, <https://doi.org/10.1126/sciadv.adr5453>, 2024.

Deng, Y., Li, P., Fang, T., Jiang, Y., Chen, J., Chen, N., Yuan, D., and Ma, J.: Automated determination of dissolved reactive phosphorus at nanomolar to micromolar levels in natural waters using a portable flow analyzer, *Anal Chem*, 92, 4379-4386, <https://doi.org/10.1021/acs.analchem.9b05252.s001>, 2020.

Dong, S., Wang, X. T., Subhas, A. V., Pavia, F. J., Adkins, J. F., and Berelson, W. M.: Depth profiles of suspended carbon and nitrogen along a North Pacific transect: Concentrations, isotopes, and ratios, *Limnol Oceanogr*, 67, 247-260, <https://doi.org/10.1002/lno.11989>, 2022.

Dong, S., Berelson, W. M., Rollins, N. E., Subhas, A. V., Naviaux, J. D., Celestian, A. J., Liu, X., Turaga, N., Kemnitz, N. J., and Byrne, R. H.: Aragonite dissolution kinetics and calcite/aragonite ratios in sinking and suspended particles in the North Pacific, *Earth Planet Sc Lett*, 515, 1-12, <https://doi.org/10.1016/j.epsl.2019.03.016>, 2019.

Eguchi, N. O., Ujiie, H., Kawahata, H., and Taira, A.: Seasonal variations in planktonic foraminifera at three sediment traps in the subarctic, transition and subtropical zones of the central North Pacific Ocean, *Mar Micropaleontol*, 48, 149-163, [https://doi.org/10.1016/S0377-8398\(03\)00020-3](https://doi.org/10.1016/S0377-8398(03)00020-3), 2003.



591 Fabry, V. J.: Aragonite production by pteropod molluscs in the subarctic Pacific, *Deep sea research I*, 36, 1735-1751,  
592 [https://doi.org/10.1016/0198-0149\(89\)90069-1](https://doi.org/10.1016/0198-0149(89)90069-1), 1989.

593 Feely, R., Sabine, C., Lee, K., Millero, F., Lamb, M., Greeley, D., Bullister, J., Key, R., Peng, T. H., and Kozyr, A.: In situ  
594 calcium carbonate dissolution in the Pacific Ocean, *Global Biogeochem Cy*, 16, 91-91-91-12,  
595 <https://doi.org/10.1029/2002gb001866>, 2002.

596 Feely, R. A., Sabine, C. L., Lee, K., Berelson, W., Kleypas, J., Fabry, V. J., and Millero, F. J.: Impact of anthropogenic CO<sub>2</sub> on  
597 the CaCO<sub>3</sub> system in the oceans, *Science*, 305, 362-366, <https://doi.org/10.1126/science.1097329>, 2004.

598 Graziano, L. M., Balch, W. M., Drapeau, D., Bowler, B. C., Vaillancourt, R., and Dunford, S.: Organic and inorganic carbon  
599 production in the Gulf of Maine, *Cont Shelf Res*, 20, 685-705, [https://doi.org/10.1016/S0278-4343\(99\)00091-6](https://doi.org/10.1016/S0278-4343(99)00091-6), 2000.

600 Gregg, W. W. and Casey, N. W.: Modeling coccolithophores in the global oceans, *Deep sea research II*, 54, 447-477,  
601 <https://doi.org/10.1016/j.dsr2.2006.12.007>, 2007.

602 Hagino, K., Okada, H., and Matsuoka, H.: Coccolithophore assemblages and morphotypes of *Emiliania huxleyi* in the  
603 boundary zone between the cold Oyashio and warm Kuroshio currents off the coast of Japan, *Mar Micropaleontol*, 55, 19-47,  
604 <https://doi.org/10.1016/j.marmicro.2005.02.002>, 2005.

605 Hartnett, A., Böttger, L. H., Matzanke, B. F., and Carrano, C. J.: Iron transport and storage in the coccolithophore: *Emiliania*  
606 *huxleyi*, *Metallomics*, 4, 1160-1166, <https://doi.org/10.1039/c2mt20144e>, 2012.

607 Hirata, T., Hardman-Mountford, N., Brewin, R., Aiken, J., Barlow, R., Suzuki, K., Isada, T., Howell, E., Hashioka, T., and  
608 Noguchi-Aita, M.: Synoptic relationships between surface Chlorophyll-a and diagnostic pigments specific to phytoplankton  
609 functional types, *Biogeosciences*, 8, 311-327, <https://doi.org/10.5194/bg-8-311-2011>, 2011.

610 Holligan, P., Charalampopoulou, A., and Hutson, R.: Seasonal distributions of the coccolithophore, *Emiliania huxleyi*, and of  
611 particulate inorganic carbon in surface waters of the Scotia Sea, *J Marine Syst*, 82, 195-205,  
612 <https://doi.org/10.1016/j.jmarsys.2010.05.007>, 2010.

613 Jin, X., Liu, C., Poulton, A. J., Dai, M., and Guo, X.: Coccolithophore responses to environmental variability in the South  
614 China Sea: species composition and calcite content, *Biogeosciences*, 13, 4843-4861, <https://doi.org/10.5194/bg-13-4843-2016>,  
615 2016.

Johns, C. T., Bondoc-Naumovitz, K. G., Matthews, A., Matson, P. G., Iglesias-Rodriguez, M. D., Taylor, A. R., Fuchs, H. L., and Bidle, K. D.: Adsorptive exchange of coccolith biominerals facilitates viral infection, *Science Advances*, 9, eadc8728, <https://doi.org/10.1126/sciadv.adc8728>, 2023.

Klaas, C. and Archer, D. E.: Association of sinking organic matter with various types of mineral ballast in the deep sea: Implications for the rain ratio, *Global Biogeochem Cy*, 16, 63-61-63-14, <https://doi.org/10.1029/2001gb001765>, 2002.

Krumhardt, K. M., Lovenduski, N. S., Iglesias-Rodriguez, M. D., and Kleypas, J. A.: Coccolithophore growth and calcification in a changing ocean, *Prog Oceanogr*, 159, 276-295, <https://doi.org/10.1016/j.pocean.2017.10.007>, 2017.

Lai, J., Zou, Y., Zhang, J., and Peres-Neto, P. R.: Generalizing hierarchical and variation partitioning in multiple regression and canonical analyses using the rdacca. hp R package, *Methods Ecol Evol*, 13, 782-788, <https://doi.org/10.1111/2041-210X.13800>, 2022.

Lam, P. J., Ohnemus, D. C., and Auro, M. E.: Size-fractionated major particle composition and concentrations from the US GEOTRACES North Atlantic Zonal Transect, *Deep sea research II*, 116, 303-320, <https://doi.org/10.1016/j.dsr2.2014.11.020>, 2015.

Lam, P. J., Lee, J.-M., Heller, M. I., Mehic, S., Xiang, Y., and Bates, N. R.: Size-fractionated distributions of suspended particle concentration and major phase composition from the US GEOTRACES Eastern Pacific Zonal Transect (GP16), *Mar Chem*, 201, 90-107, <https://doi.org/10.1016/j.marchem.2017.08.013>, 2018.

Li, Y., Meng, F., Wang, B., Yang, M., Liu, C.-Q., and Xu, S.: Regulation of particulate inorganic carbon by phytoplankton in hydropower reservoirs: Evidence from stable carbon isotope analysis, *Chem Geol*, 579, 120366, <https://doi.org/10.1016/j.chemgeo.2021.120366>, 2021.

Lohbeck, K. T., Riebesell, U., and Reusch, T. B.: Adaptive evolution of a key phytoplankton species to ocean acidification, *Nat Geosci*, 5, 346-351, <https://doi.org/10.1038/ngeo1441>, 2012.

Ma, D., Gregor, L., and Gruber, N.: Four decades of trends and drivers of global surface ocean acidification, *Global Biogeochem Cy*, 37, e2023GB007765, <https://doi.org/10.1029/2023GB007765>, 2023.

Maranón, E., Balch, W. M., Cermeno, P., González, N., Sobrino, C., Fernández, A., Huete-Ortega, M., López-Sandoval, D. C., Delgado, M., and Estrada, M.: Coccolithophore calcification is independent of carbonate chemistry in the tropical ocean,

641 Limnol Oceanogr, 61, 1345-1357, <https://doi.org/10.1002/lno.10295>, 2016.

642 Naviaux, J. D., Subhas, A. V., Rollins, N. E., Dong, S., Berelson, W. M., and Adkins, J. F.: Temperature dependence of calcite  
643 dissolution kinetics in seawater, Geochim Cosmochim Acta, 246, 363-384, <https://doi.org/10.1016/j.gca.2018.11.037>, 2019.

644 Neukermans, G., Bach, L., Butterley, A., Sun, Q., Claustre, H., and Fournier, G.: Quantitative and mechanistic understanding  
645 of the open ocean carbonate pump-perspectives for remote sensing and autonomous in situ observation, Earth-Science Reviews,  
646 239, 104359, <https://doi.org/10.1016/j.earscirev.2023.104359>, 2023.

647 O'Brien, C. J., Vogt, M., and Gruber, N.: Global coccolithophore diversity: Drivers and future change, Prog Oceanogr, 140,  
648 27-42, <https://doi.org/10.1016/j.pocean.2015.10.003>, 2016.

649 Okada, H. and Honjo, S.: The distribution of oceanic coccolithophorids in the Pacific, Deep Sea Research and Oceanographic  
650 Abstracts, 355-374, [https://doi.org/10.1016/0011-7471\(73\)90059-4](https://doi.org/10.1016/0011-7471(73)90059-4), 1973.

651 Oksanen, J.: Vegan: community ecology package, <http://vegan.r-forge.r-project.org/>, 2010.

652 Poulton, A., Sanders, R., Holligan, P., Stinchcombe, M., Adey, T., Brown, L., and Chamberlain, K.: Phytoplankton  
653 mineralization in the tropical and subtropical Atlantic Ocean, Global Biogeochem Cy, 20,  
654 <https://doi.org/10.1029/2006gb002712>, 2006.

655 Poulton, A. J., Holligan, P. M., Charalampopoulou, A., and Adey, T. R.: Coccolithophore ecology in the tropical and subtropical  
656 Atlantic Ocean: New perspectives from the Atlantic meridional transect (AMT) programme, Prog Oceanogr, 158, 150-170,  
657 <https://doi.org/10.1016/j.pocean.2017.01.003>, 2017.

658 Poulton, A. J., Painter, S. C., Young, J. R., Bates, N. R., Bowler, B., Drapeau, D., Lyczskowski, E., and Balch, W. M.: The  
659 2008 *Emiliana huxleyi* bloom along the Patagonian Shelf: Ecology, biogeochemistry, and cellular calcification, Global  
660 Biogeochem Cy, 27, 1023-1033, <https://doi.org/10.1002/2013gb004641>, 2013.

661 Quere, C. L., Harrison, S. P., Colin Prentice, I., Buitenhuis, E. T., Aumont, O., Bopp, L., Claustre, H., Cotrim Da Cunha, L.,  
662 Geider, R., and Giraud, X.: Ecosystem dynamics based on plankton functional types for global ocean biogeochemistry models,  
663 Global Change Biol, 11, 2016-2040, <https://doi.org/10.1111/j.1365-2486.2005.1004.x>, 2005.

664 Raven, J. A. and Crawford, K.: Environmental controls on coccolithophore calcification, Mar Ecol Prog Ser, 470, 137-166,  
665 <https://doi.org/10.3354/meps09993>, 2012.

Rickaby, R., Monteiro, F., Bach, L., Brownlee, C., Bown, P., Poulton, A., Beaufort, L., Dutkiewicz, S., Gibbs, S., and Gutowska, M.: Why marine phytoplankton calcify, *Science Advances*, 2, <https://doi.org/10.1126/sciadv.1501822>, 2016a.

Rickaby, R. E., Hermoso, M., Lee, R. B., Rae, B. D., Heures, A. M., Balestreri, C., Chakravarti, L., Schroeder, D. C., and Brownlee, C.: Environmental carbonate chemistry selects for phenotype of recently isolated strains of *Emiliana huxleyi*, *Deep sea research II*, 127, 28-40, <https://doi.org/10.1016/j.dsr2.2016.02.010>, 2016b.

Rigual Hernández, A. S., Trull, T. W., Nodder, S. D., Flores, J. A., Bostock, H., Abrantes, F., Eriksen, R. S., Sierro, F. J., Davies, D. M., and Ballegeer, A.-M.: Coccolithophore biodiversity controls carbonate export in the Southern Ocean, *Biogeosciences*, 17, 245-263, <https://doi.org/10.5194/bg-17-245-2020>, 2020.

Rivero-Calle, S., Gnanadesikan, A., Del Castillo, C. E., Balch, W. M., and Guikema, S. D.: Multidecadal increase in North Atlantic coccolithophores and the potential role of rising CO<sub>2</sub>, *Science*, 350, 1533-1537, <https://doi.org/10.1126/science.aaa8026>, 2015.

Rousseaux, C. S. and Gregg, W. W.: Recent decadal trends in global phytoplankton composition, *Global Biogeochem Cy*, 29, 1674-1688, <https://doi.org/10.1002/2015gb005139>, 2015.

Saavedra-Pellitero, M., Baumann, K.-H., Flores, J.-A., and Gersonde, R.: Biogeographic distribution of living coccolithophores in the Pacific sector of the Southern Ocean, *Mar Micropaleontol*, 109, 1-20, <https://doi.org/10.1016/j.marmicro.2014.03.003>, 2014.

Schiebel, R., Spielhagen, R. F., Garnier, J., Hagemann, J., Howa, H., Jentzen, A., Martínez-García, A., Meilland, J., Michel, E., and Repschläger, J.: Modern planktic foraminifers in the high-latitude ocean, *Mar Micropaleontol*, 136, 1-13, <https://doi.org/10.1016/j.marmicro.2017.08.004>, 2017.

Schlüter, L., Lohbeck, K. T., Gutowska, M. A., Gröger, J. P., Riebesell, U., and Reusch, T. B.: Adaptation of a globally important coccolithophore to ocean warming and acidification, *Nat Clim Change*, 4, 1024-1030, <https://doi.org/10.1038/nclimate2379>, 2014.

Sheward, R. M., Poulton, A. J., Young, J. R., de Vries, J., Monteiro, F. M., and Herrle, J. O.: Cellular morphological trait dataset for extant coccolithophores from the Atlantic Ocean, *Scientific Data*, 11, 720, <https://doi.org/10.1038/s41597-024-03544-1>, 2024.

691 Sinha, B., Buitenhuis, E. T., Le Quéré, C., and Anderson, T. R.: Comparison of the emergent behavior of a complex ecosystem  
 692 model in two ocean general circulation models, *Prog Oceanogr*, 84, 204-224, <https://doi.org/10.1016/j.pocean.2009.10.003>,  
 693 2010.

694 Smith, S. V. and Mackenzie, F. T.: The role of CaCO<sub>3</sub> reactions in the contemporary oceanic CO<sub>2</sub> cycle, *Aquat Geochem*,  
 695 22, 153-175, <https://doi.org/10.1007/s10498-015-9282-y>, 2016.

696 Subhas, A. V., Dong, S., Naviaux, J. D., Rollins, N. E., Ziveri, P., Gray, W., Rae, J. W., Liu, X., Byrne, R. H., and Chen, S.:  
 697 Shallow calcium carbonate cycling in the North Pacific Ocean, *Global Biogeochem Cy*, 36, e2022GB007388,  
 698 <https://doi.org/10.7185/gold2021.4474>, 2022.

699 Sugie, K. and Suzuki, K.: Characterization of the synoptic-scale diversity, biogeography, and size distribution of diatoms in  
 700 the North Pacific, *Limnol Oceanogr*, 62, 884-897, <https://doi.org/10.1002/lno.10473>, 2017.

701 Takahashi, T., Sutherland, S. C., Wanninkhof, R., Sweeney, C., Feely, R. A., Chipman, D. W., Hales, B., Friederich, G., Chavez,  
 702 F., and Sabine, C.: Climatological mean and decadal change in surface ocean pCO<sub>2</sub>, and net sea–air CO<sub>2</sub> flux over the global  
 703 oceans, *Deep sea research II*, 56, 554-577, <https://doi.org/10.1016/j.dsr2.2008.12.009>, 2009.

704 Taylor, A. R., Brownlee, C., and Wheeler, G.: Coccolithophore cell biology: chalking up progress, *Annu Rev Mar Sci*, 9, 283-  
 705 310, <https://doi.org/10.1146/annurev-marine-122414-034032>, 2017.

706 Taylor, B. J., Rae, J. W., Gray, W. R., Darling, K. F., Burke, A., Gersonde, R., Abelman, A., Maier, E., Esper, O., and Ziveri,  
 707 P.: Distribution and ecology of planktic foraminifera in the North Pacific: Implications for paleo-reconstructions, *Quaternary*  
 708 *Sci Rev*, 191, 256-274, <https://doi.org/10.1016/j.quascirev.2018.05.006>, 2018.

709 Vincent, F., Gralka, M., Schleyer, G., Schatz, D., Cabrera-Brufau, M., Kuhlisch, C., Sichert, A., Vidal-Melgosa, S., Mayers,  
 710 K., Barak-Gavish, N., Flores, J. M., Masdeu-Navarro, M., Egge, J. K., Larsen, A., Hehemann, J.-H., Marrasé, C., Simó, R.,  
 711 Cordero, O. X., and Vardi, A.: Viral infection switches the balance between bacterial and eukaryotic recyclers of organic matter  
 712 during coccolithophore blooms, *Nat Commun*, 14, 510, <https://doi.org/10.1038/s41467-023-36049-3>, 2023.

713 Volk, T. and Hoffert, M. I.: Ocean carbon pumps: Analysis of relative strengths and efficiencies in ocean-driven atmospheric  
 714 CO<sub>2</sub> changes, *The carbon cycle and atmospheric CO<sub>2</sub>: Natural variations Archean to present*, 32, 99-110,  
 715 <https://doi.org/10.1029/gm032p0099>, 1985.

Welschmeyer, N. A.: Fluorometric analysis of chlorophyll a in the presence of chlorophyll b and pheopigments, *Limnol Oceanogr*, 39, 1985-1992, <https://doi.org/10.4319/lo.1994.39.8.1985>, 1994.

Yang, T.-N. and Wei, K.-Y.: How many coccoliths are there in a coccosphere of the extant coccolithophorids? A compilation, *Br. Phycol. J*, 26, 67-80, <https://doi.org/10.58998/jnr2275>, 2003.

Young, J., Geisen, M., Cros, L., Kleijne, A., Sprengel, C., Probert, I., and Østergaard, J.: A guide to extant coccolithophore taxonomy, *Journal of Nannoplankton Research*, 1, 1-132, <https://doi.org/10.58998/jnr2297>, 2003.

Coccobiom2 Macros, available at: [ina.tmsoc.org/nannos/coccobiom/Usernotes.html](http://ina.tmsoc.org/nannos/coccobiom/Usernotes.html): <http://ina.tmsoc.org/nannos/coccobiom/Usernotes.html>, last

Young, J. R. and Ziveri, P.: Calculation of coccolith volume and its use in calibration of carbonate flux estimates, *Deep sea research II*, 47, 1679-1700, [https://doi.org/10.1016/s0967-0645\(00\)00003-5](https://doi.org/10.1016/s0967-0645(00)00003-5), 2000.

Zhang, J.-Z.: Shipboard automated determination of trace concentrations of nitrite and nitrate in oligotrophic water by gas-segmented continuous flow analysis with a liquid waveguide capillary flow cell, *Deep sea research I*, 47, 1157-1171, [https://doi.org/10.1016/s0967-0637\(99\)00085-0](https://doi.org/10.1016/s0967-0637(99)00085-0), 2000.

Zhu, Y., Yuan, D., Huang, Y., Ma, J., and Feng, S.: A sensitive flow-batch system for on board determination of ultra-trace ammonium in seawater: Method development and shipboard application, *Anal Chim Acta*, 794, 47-54, <https://doi.org/10.1016/j.aca.2013.08.009>, 2013.

Zhu, Y., Liu, J., Huang, T., Wang, L., Trull, T. W., and Dai, M.: On the fluorometric measurement of ammonium in oligotrophic seawater: Assessment of reagent blanks and interferences, *Limnol Oceanogr-Meth*, 16, 516-524, <https://doi.org/10.1002/lom3.10263>, 2018.

Ziveri, P., de Bernardi, B., Baumann, K.-H., Stoll, H. M., and Mortyn, P. G.: Sinking of coccolith carbonate and potential contribution to organic carbon ballasting in the deep ocean, *Deep sea research II*, 54, 659-675, <https://doi.org/10.1016/j.dsr2.2007.01.006>, 2007.

Ziveri, P., Gray, W. R., Anglada-Ortiz, G., Manno, C., Grelaud, M., Incarbona, A., Rae, J. W. B., Subhas, A. V., Pallacks, S., and White, A.: Pelagic calcium carbonate production and shallow dissolution in the North Pacific Ocean, *Nat Commun*, 14, 805, <https://doi.org/10.1038/s41467-023-36177-w>, 2023.